© 2022. Published by The Company of Biologists Ltd | Development (2022) 149, dev199974. doi:10.1242/dev.199974

RESEARCH ARTICLE

A unique miR775-*GALT9* module regulates leaf senescence in *Arabidopsis* during post-submergence recovery by modulating ethylene and the abscisic acid pathway

Vishnu Mishra[1,‡], Archita Singh[1,2,‡], Nidhi Gandhi[1], Shabari Sarkar Das[2,3], Sandeep Yadav[1], Ashutosh Kumar[1] and Ananda K. Sarkar[1,2,*,§]

ABSTRACT

The submergence-induced hypoxic condition negatively affects the plant growth and development, and causes early onset of senescence. Hypoxia alters the expression of a number of microRNAs (miRNAs). However, the molecular function of submergence stress-induced miRNAs in physiological or developmental changes and recovery remains poorly understood. Here, we show that miR775 is an *Arabidopsis thaliana*-specific young and unique miRNA that possibly evolved non-canonically. miR775 post-transcriptionally regulates *GALACTOSYLTRANSFERASE 9* (*GALT9*) and their expression is inversely affected at 24 h of complete submergence stress. The overexpression of miR775 (miR775-Oe) confers enhanced recovery from submergence stress and reduced accumulation of *RBOHD* and ROS, in contrast to wild-type and *MIM775 Arabidopsis* shoot. A similar recovery phenotype in the *galt9* mutant indicates the role of the miR775-*GALT9* module in post-submergence recovery. We predicted that Golgi-localized GALT9 is potentially involved in protein glycosylation. The altered expression of senescence-associated genes (*SAG12*, *SAG29* and *ORE1*), ethylene signalling (*EIN2* and *EIN3)* and abscisic acid (ABA) biosynthesis (*NCED3*) pathway genes occurs in miR775-Oe, *galt9* and *MIM775* plants. Thus, our results indicate the role for the miR775-*GALT9* module in post-submergence recovery through a crosstalk between the ethylene signalling and ABA biosynthesis pathways.

KEY WORDS: miRNA, miR775, *GALT9*, Senescence, Submergence stress, Hypoxia, SAG genes, *Arabidopsis*

INTRODUCTION

Abiotic factors, such as light, temperature, water, oxygen, nutrition, etc., act as external cues to modulate plant growth and development (Kraehmer, 2016). Globally, flood is one of the major stresses that lead to severe loss of crop yield and productivity (Ismail, 2018; Kumar and Dash, 2019; Bui et al., 2020). Flooding stress is divided into two categories depending upon the water exposure: complete submergence and partial submergence (or waterlogging). Under complete submergence, the whole plant is fully immersed in water; under partial submergence, the shoot terminal is maintained above the water surface (Fukao et al., 2019). Premature senescence, necrosis, chlorosis and cessation of growth are the major consequences of submergence stress (Zhang et al., 2000; Visser et al., 2003). Submergence initiates various molecular cascades that adversely affect plant growth and development. Submergence also leads to excessive reactive oxygen species (ROS) production and cell death, due to the reduced availability of oxygen (hypoxic conditions). Prolonged submergence gradually affects gaseous exchange, which leads to cell damage and chlorophyll breakdown causing early onset of senescence (Fukao et al., 2019). *RESPIRATORY BURST OXIDASE HOMOLOGUE D* (*RBOHD*) is one of the NAPDH oxidases involved in the production of ROS and is widely used as a marker gene to assess ROS accumulation during submergence stress. *RBOHD* promotes the expression of alcohol dehydrogenase (ADH), pyruvate decarboxylase 1 (PDC), lactate dehydrogenase (LDH), calcium (Ca^{2+}) levels and various hypoxia-responsive genes, induced during hypoxia stress. An abundance of *RBOHD* also changes under submergence due to oxidative stress (Yamauchi et al., 2013; Yeung et al., 2018). Senescence-associated genes (SAGs), such as *SAG12*, *SAG29* and *ORESARA1* (*ORE1/NAC6*) are mainly expressed in senescent tissue, which ultimately leads to chlorophyll breakdown and leaf senescence. *SAG12* encodes a cysteine protease (vacuolar protein) in *Arabidopsis thaliana* (*Arabidopsis*) and is associated with oxidative stress (H_2O_2) and senescence (Weaver et al., 1998). Increased *SAG12* transcript levels lead to early leaf senescence in *Arabidopsis* (Ding et al., 2016; Ueda et al., 2020). Similarly, *SAG29* is also prominently expressed in senescing plant tissue and its expression is increased by osmotic stresses through an abscisic acid (ABA)-dependent pathway (Seo et al., 2011). *ORE1* has been identified as an accession-specific regulatory gene that is expressed at high levels in the Bay-0 ecotype (an *Arabidopsis* accession) and has a predominant role in chlorophyll breakdown. The *ore1* mutant showed intermediary submergence tolerance (Yeung et al., 2018). Both *ORE1* and *SAG29* accelerate leaf senescence in *Arabidopsis* (Kim et al., 2009; Qiu et al., 2015; Zhang et al., 2018).

Besides genes and transcription factors (TFs), a large number of miRNAs have been also reported to be dynamically regulated under submergence stress (Zhang et al., 2008; Moldovan et al., 2010; Licausi et al., 2011; Liu et al., 2012; Jeong et al., 2013; Zhai et al., 2013; Jin et al., 2017; Li et al., 2017; Franke et al., 2018; Fukao et al., 2019). MicroRNAs (miRNAs) belong to a class of endogenous small non-coding RNAs that negatively regulate their target gene expression at the post-transcriptional level through

[1]National Institute of Plant Genome Research, Aruna Asaf Ali Marg, New Delhi 110067, India. [2]School of Life Sciences, Jawaharlal Nehru University, New Delhi 110067, USA. [3]Department of Botany and Forestry, Vidyasagar University, Midnapore, West Bengal 721104, India.
*Present address: School of Life Sciences, Jawaharlal Nehru University, New Delhi 110067, India.
‡These authors contributed equally to this work

§Author for correspondence (aksarkar@nipgr.ac.in; anandaksarkar@mail.jnu.ac.in)

V.M., 0000-0002-0826-3580; A.S., 0000-0003-0116-6267; S.S.D., 0000-0001-7952-7531; S.Y., 0000-0001-8858-4271; A.K., 0000-0002-1699-2951; A.K.S., 0000-0001-7169-4298

Handling Editor: Ykä Helariutta
Received 5 July 2021; Accepted 6 December 2021

Development (2022) 149, dev199974. doi:10.1242/dev.199974

complementary pairing with their specific target mRNAs in most of the eukaryotes. Several miRNAs have recently been implicated in various developmental processes, including shoot and root development. Many miRNAs have been shown to be differentially expressed under various abiotic stress conditions (Singh et al., 2020a; Wang et al., 2020).

Previous reports showed the involvement of some miRNAs in the regulation of SAG genes, e.g. miR164-mediated regulation of *ORE1* triggers early senescence by regulating various SAG genes (Balazadeh et al., 2010; Glazińska et al., 2014; Yeung et al., 2018). miR159 was found to be upregulated in maize root during waterlogging or flood conditions and its targets, gibberellin-mediated expression of myeloblastosis genes (GAMYBs; e.g. *MYB33* and *MYB101*) were downregulated (Liu et al., 2012). miR166 is shown to have an important role in response to flood stress through regulating calcium spikes and accumulation of ROS during root growth and development (Fukao et al., 2019). miR167 was found to regulate short-term waterlogging or submergence in maize root by targeting auxin response factors (ARFs) (Zhang et al., 2008; Liu et al., 2012). Recently, a report showed that miR167 was differentially upregulated in *Alternanthera philoxeroides* and *Populus tomentosa* plants during flood response (Li et al., 2017). Moreover, miR156 have been indicated for its potential role in submergence and hypoxia by targeting squamosa promoter binding protein-likes genes (SPLs) in lotus and *Arabidopsis* (Moldovan et al., 2010; Jin et al., 2017; Franke et al., 2018). Long-term waterlogging downregulated the expression of miR172, leading to accumulation of target *AP2/ERF* mRNAs and thereby promoting crown root development in maize (Zhai et al., 2013). The expression of miR775, which targets *GALT9*, was reported to be induced by hypoxic conditions caused by flood or high altitude in *Arabidopsis* (Moldovan et al., 2010; Liu et al., 2012; Jin et al., 2017; Tripathi et al., 2019). However, the functional role of miR775 in hypoxia remains to be understood. In the present study, we have addressed the potential role of the miR775-*GALT9* module in submergence stress-induced hypoxia and post-submergence recovery in *Arabidopsis*. Our study shows that miR775-*GALT9* module plays an important role in post-submergence recovery and senescence in *Arabidopsis*, by modulating the expression of SAG genes, *RBOHD*, ethylene and ABA pathway genes.

RESULTS

Gene structure of *MIR775A* and its possible origin through promoter acquisition

MIR775A (AT1G78206) and its mature miRNA miR775, are uniquely present in *Arabidopsis*, at chromosome 1 (Araport11; with gene coordinate Chr1:29422452-29422574). Interestingly, we did not find any promoter elements in the upstream [transcription starts site (TSS) and TATA-box] of *MIR775A* up to the next gene (*snoRNA*). Hence, we searched for the existence of a canonical promoter element upstream of the *MIR775A* and *snoRNA* genes. We retrieved an intergenic sequence upstream of *MIR775A* to identify or predict the promoter through software 'TSSPlant' (http://www.softberry.com/cgi-bin/programs/promoter/tssplant.pl). We found an adjacent gene, *snoRNA* (AT1G09787.1), situated very closely (92 bp apart) in the upstream of *MIR775A*, having no predicted TSS or TATA-box (Fig. 1A). Therefore, we extended our search for the intergenic sequence between the next upstream gene, AT1G78200 (upstream of *MIR775A*). We retrieved an intergenic sequence of 587 bp, including the 3′ UTR of the AT1G78200 gene, which also overlapped with the *snoRNA* sequence, and then predicted the TSS and TATA-box elements. (Fig. 1A). TSSPlant predicted two TSS: one without a TATA box and another with a TATA box (Fig. S1A). The predicted TSS with a higher score (1.9844), which also possessed a TATA box, was considered to be the most likely candidate (Fig. S1A). This result suggests that *MIR775A* putatively acquires the promoter elements to become functional, which correlates with earlier findings that promoter acquisition is also one of the modes of evolution of miRNAs (Lu, 2019). However, we also checked other canonical modes of miRNA evolution to understand the origin of *MIR775A* in *Arabidopsis*. To address this, we first investigated whether *MIR775A* originated canonically through inverted duplication of its target (Allen et al., 2004). We observed that *MIR775A* and its validated target *GALT9* genes are not situated in tandem, as they are 9.55 Mbp apart from each other in chromosome 1 of the *Arabidopsis* genome (Fig. 1B), and possess no duplicated fragment, which rules out their possible origin through an inverted duplication mode, unlike common miRNAs. Furthermore, we also checked the sequence variability at the miR775-binding site in *GALT9* of *Arabidopsis* against *GALT9* orthologs (Fig. S1B). We found a highly conserved miR775-binding site in *GALT9* orthologs (Fig. S1B), which excludes the possibility that *MIR775A* originated from *GALT9*. Therefore, our analysis indicates that the *MIR775A* possibly originated specifically in the genome of *Arabidopsis* non-canonically through acquisition of a TSS and TATA box in its upstream region (Fig. 1A), which is a unique feature of miR775.

Non-conserved miR775 targets conserved *GALT9*

During our ongoing work, other studies recently validated *GALT9* as a target of ath-miR775 in *Arabidopsis* (Fahlgren et al., 2007; Mishra et al., 2021; Zhang et al., 2021). Some more targets, *DCL1* (AT1G01040), *WRKY19* (AT4G12020) and *KFB* (*KELCH DOMAIN-CONTAINING F-BOX PROTEIN*, AT1G23390) were also predicted but not validated (Zhang et al., 2011). *GALT9* achieved the status of a bona fide target of miR775; surprisingly, however, studies differed in terms of its cleavage site(s) (Fig. 1C). Our degradome analysis of the most recent TAIR database (AraPort11) using the CleaveLand tool confirmed *GALT9* as the strongest target of miR775 in *Arabidopsis*. Variable cumulative scores for a perfect cleavage site (10th) were obtained during degradome analysis in 11-day-old seedling and leaf (Fig. 1C, Tables S1 and S2). In seedling tissue, we observed the perfect cleavage site of miR775 in *GALT9* mRNA (position 10th), where all reads fell to CleaveLand analysis category (CAC) zero (0), the best score. However, in leaf, the miR775-mediated cleavage of *GALT9* appeared in CAC (2), suggesting moderate deviation from the perfect cleavage site in some aligned reads (Fig. 1C). Our results indicate tissue-specific variation of miR775-mediated cleavage of *GALT9* (Fig. 1C, Tables S1 and S2). Thus non-conserved miR775 is uniquely present specifically in *Arabidopsis*; however, its target *GALT9* and *GALT9* orthologues are widespread and conserved across the plant species (Fig. S1B).

The expression pattern in the co-infiltration experiment and in mutants or transgenics revealed negative regulation of *GALT9* by miR775

To further validate the transcriptional cleavage of *GALT9* by miR775, 4-week-old *Nicotiana benthamiana* (tobacco) leaves were co-infiltrated with the construct *35S:GALT9-GFP* (control), with empty vector (EV)+*35S:GALT9-GFP*, and with *35S:MIR775A+35S:GALT9-GFP* (Fig. S2A). If cleaving *GALT9*, co-infiltrated miR775 should cleave the *GALT9* transcripts and reduce the expression of *GFP*. In parallel, we used another miRNA, miR839, as an additional

Development (2022) 149, dev199974. doi:10.1242/dev.199974

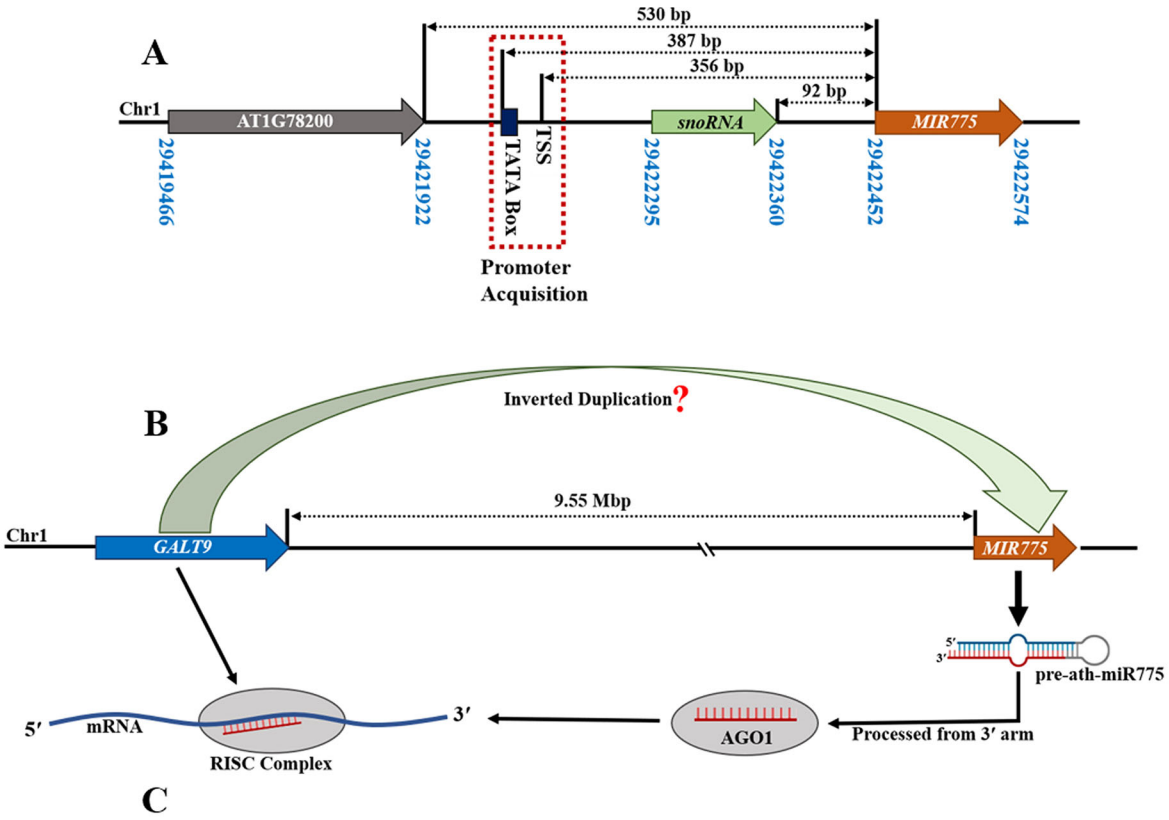

ath-miR775 and its target binding site		Cleavage site	Type of Analysis	Reference
GALT9 5' UCGUACUGCUAGAUAUCGAA 3' Ath-miR775 3' ACCGUGACGAUCUGUAGCUU 5'		10^{th} – $12^{\#}$/0* in Seedling 10^{th} – $5^{\#}$/2* in leaf	Degradome	Present study
Ath-miR775 ACCGUGACGAUCUGUAGCUU-5′ *GALT9* 5′-UUCGUACUGCUAGAUAUCGAA		14^{th} – 5/20 15^{th} – 9/20	5′ RLM-RACE	Zhang et. al., 2021
GALT9 5′ UCGUACUGCUAGAUAUCGAA 3′ Ath-miR775 3′ ACCGUGACGAUCUGUAGCUU 5′		10^{th} – 9/12	5′ RLM-RACE	Mishra et. al., 2021
GALT9 5′ CUUCGUACUGCUAGAUAUCGAAGA 3′ Ath-miR775 3′ ACCGUGACGAUCUGUAGCUU 5′		10^{th} – 1/21	5′ RLM-RACE	Fahlgren et. al., 2007

*Number of Reads; *Cleaveland analysis category, lowest value is better

Fig. 1. The structure, possible origin and functional annotation of *MIR775A*. (A) Gene structure of *MIR775A* in *Arabidopsis*, where the presence of a predicted TSS and TATA box shows putative promoter (acquisition) in the upstream region. Numbers in blue represent gene coordinates at chromosome 1. (B) Putative mode of origin and processing of mature miR775. (C) Comparative studies showing the variation of miR775 target cleavage sites in *GALT9* transcripts in *Arabidopsis*. *CleaveLand analysis category. #Number of reads in the degradome dataset cleaved at the 10th position of miR775.

control to validate that the *GALT9* is specifically targeted by miR775 and co-infiltrated the tobacco leaves with *35S:MIR839A+35S:GALT9-GFP*. Furthermore, we quantified the level of *GFP* by quantitative RT-PCR (qRT-PCR) (Fig. S2B) and observed significant reduction in co-infiltrated (*35S:MIR775A* and *35S:GALT9:GFP*) tobacco leaves in comparison with tobacco leaf co-infiltrated with *35S:GALT9-GFP*, *EV+35S:GALT9-GFP* and *35S:MIR839A+35S:GALT9-GFP*. Reduced expression of *GFP* confirmed the post-transcriptional cleavage of *GALT9* transcripts by miR775 (Fig. S2B). To further confirm the miR775-mediated downregulation of *GALT9* in *Arabidopsis*, we analysed the expression of *GALT9* in two independent miR775-overexpression lines (miR775-Oe1 and miR775-Oe2) (Fig. 2A) and observed its reduced expression (by 48% and 63%, respectively) (Fig. 2B). Furthermore, we observed significant upregulation of *GALT9* transcript level in two independent lines with a target mimic of miR775 (*MIM775-1* and *MIM775-2*) by 3.98- and 2.55-fold, respectively (Fig. 2C). These results confirmed the post-transcriptional regulation of *GALT9* by miR775, which is consistent with a recent study (Zhang et al., 2021) published during the processing of this article.

Functional annotation by GALT9 protein structure analysis

The 3D structure of GALT9 was predicted using I-TASSER, which further deduces protein functions and biological annotations. We analysed the enzyme commission (EC) numbers and gene ontology (GO) terms, and annotated their putative molecular function based on modelled 3D structure of GALT9. The best consensus putative function of GALT9 is that of an enzyme, β-1,3-galactosyl-O-

Development (2022) 149, dev199974. doi:10.1242/dev.199974

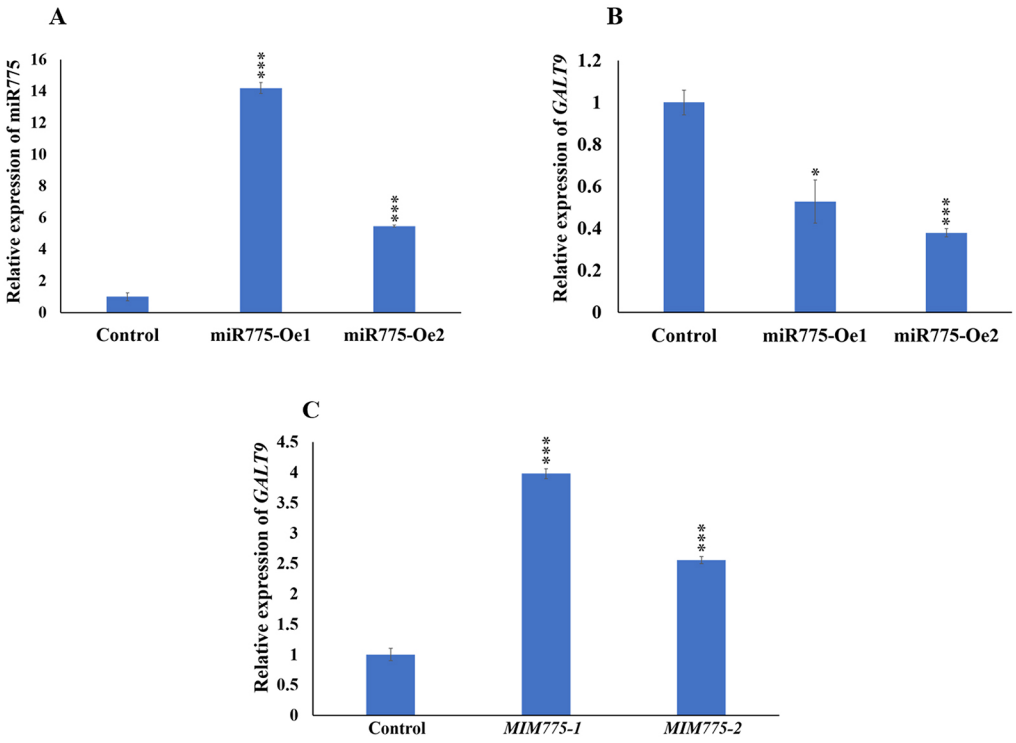

Fig. 2. Relative expression of miRNAs and their target (*GALT9*). (A) Relative quantification of miR775 expression in miR775-Oe1 and miR775-Oe2. (B) Relative expression of *GALT9* in miR775-Oe1 and miR775-Oe2. (C) Relative expression of *GALT9* in *MIM775-1* and *MIM775-2*. Data are mean±s.e.m. of three independent experiments. Asterisks indicate significant statistical differences (***$P \leq 0.001$ and *$P \leq 0.05$, two-tailed Student's *t*-test).

glycosyl-glycoprotein β-1,6-N-acetylglucosaminyltransferase (EC number: 2.4.1.102). GALT9 has a role in protein glycosylation (GO:0006486), where the ligand is uridine-diphosphate (UDP), which is involved in UDP-glycosyltransferase activity (GO:0008194), and is localized in Golgi membrane (GO:0000139) (Figs S4 and S5). These results indicate that GALT9 is involved in the transfer of glycosyl groups (GO:0016757) to protein moieties (e.g. the addition of glycan chains to proteins) through peptidyl-asparagine modification (GO:0018196). The peptidyl-asparagine modification helps in N-glycosylation, where glycans are attached to the side-chain nitrogen atoms of asparagine (Asn) residues in a conserved consensus sequence asparagine-Xaa-serine/threonine (Asn-Xaa-Ser/Thr), where Xaa could be any amino acid (Schwarz and Aebi, 2011).

Arabidopsis GALT9 is a member of the Carbohydrate Active Enzyme (*CAZy*) family and the protein localizes in Golgi apparatus

The coding sequence of *GALT9* consists of 1038 bp, including seven exons that are interrupted by six introns while GALT9 proteins consist of 345 amino acid residues (https://www.arabidopsis.org/servlets/TairObject?name=AT1G53290&type=locus). GALT9 protein catalyzes the transfer of a glycosyl group from a UDP-glycosyl donor molecule to protein moieties (Qu et al., 2008; Gille et al., 2013; Qin et al., 2013). *Arabidopsis* GALT9 shows strong homology with *Gossypium hirsutum* (cotton) GhGALT1 and belongs to the Carbohydrate Active Enzyme glycosyltransferases (CAZy GT) family (Qin et al., 2013). A total 31 members of the CAZy GT-family are present in *Arabidopsis* and, out of 31, 20 members have a β-(1-3)-GT motif, similar to mammalian systems (Qu et al., 2008). As GALT9 is potentially involved in post-translational modification of proteins, we investigated its subcellular localization. Using the *Arabidopsis* Subcellular Localization Prediction Server (AtSubP, http://bioinfo3.noble.org/AtSubP/index.php), we predicted GALT9 protein was localized in the Golgi apparatus, at a subcellular level. To validate this, we generated a translation fusion reporter (*35S:GALT9-GFP*) construct and co-infiltrated it with a *GmManI*-pBIN2 Golgi mCherry marker for transient subcellular localization in *Nicotiana benthamiana* leaves. Using differential interference contrast (DIC) microscopy analysis, we found fluorescence from *35S:GALT9-GFP* to be primarily localized in the Golgi apparatus which is consistent with a recently published study (Zhang et al., 2021), further validating the *in silico* prediction (Fig. S5).

MIR775A and target *GALT9* showed complementary and dynamic expression pattern predominantly in shoot and root tissues

To investigate the spatiotemporal expression pattern of *MIR775A* and its target *GALT9*, we performed the histochemical GUS assay in 5 days after germination (dag) seedlings and in 35-day-old *pMIR775A:GUS* and *pGALT9:GUS* plants. In 5 dag seedlings, *MIR775A* showed expression in the shoot, hypocotyl, cotyledons, leaves, root-shoot junction (RSJ), stomata, trichomes and rosette leaves of 35-day-old plants (Fig. 3A-E). *GALT9* was also expressed in shoot, root-shoot junction, hypocotyl, leaves, stomata and trichomes in 5 dag seedlings and in rosette leaves of 35-day-old plants (Fig. 3F-J). The GUS expression of *pMIR775A:GUS* and *pGALT9:GUS* was moderately complementary in shoot, shoot apex, root-shoot junction, hypocotyl, stomata, trichome and rosette leaves.

Furthermore, we quantified and compared the expression level among 5 dag whole seedlings, shoot and roots (Fig. 4A), which showed higher expression of *MIR775A* in shoot when compared with root (Fig. 4A). *MIR775A* and *GALT9* showed complementary expression in young rosette, cauline leaves and flower (Fig. 4B). The availability of mature miRNA depends on many factors, such as the activity of miRNA biosynthesis pathway genes, miRNA processing machinery, etc. (Chen, 2009). Therefore, we also validated the accumulation of functional mature miRNA in different tissues of 35-day-old Col-0 plants by stem-loop qRT-

Development (2022) 149, dev199974. doi:10.1242/dev.199974

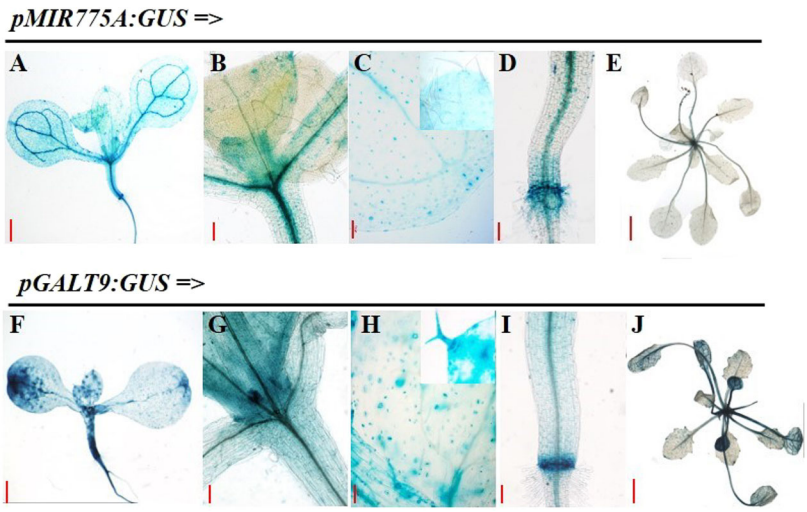

Fig. 3. Tissue-specific expression pattern of *MIR775A* and its target, *GALT9*, in *Arabidopsis thaliana*. (A-E) GUS expression of *MIR775A* in seedlings 5 days after germination (dag). Representation of expressions in different tissues are as follows: (A) shoot, (B) shoot apex, (C) cotyledon leaf, (D) root-shoot junction, and (E) 35 dag rosette leaf. (F-J) GUS expression of the target *GALT9* in (F) shoot, (G) shoot apex, (H) cotyledon leaf, (I) root and shoot junction, and (J) 35 dag rosette leaf. *n*=15. Scale bars: 100 µm.

PCR. The mature miR775 was expressed abundantly in a young rosette, young cauline, floral bud and flowers (Fig. 4B). These results suggest a dynamic spatiotemporal expression pattern of miR775 and its target *GALT9* in *Arabidopsis*, which is likely to have an impact on its physiological or developmental role.

Submergence stress affects the expression of miR775 and *GALT9* in *Arabidopsis* seedlings

Hypoxia stress conditions, caused by flooding or high altitude, are known to induce the expression of miR775 in *Arabidopsis* (Moldovan et al., 2010; Liu et al., 2012; Jin et al., 2017; Tripathi et al., 2019). To understand the molecular basis of this, we first studied the effect of submergence-induced hypoxia stress on the expression of miR775 and its target gene *GALT9* in *Arabidopsis* shoot. To analyse the submergence-induced expression of *MIR775A*, we treated 7 dag seedlings with complete submergence and analysed the expression of miR775 by stem-loop qRT-PCR and of *GALT9* transcripts by qRT-PCR at four different time points (4 h, 8 h, 12 h and 24 h) (Fig. 5A). We found that the expression of miR775 was upregulated by fivefold; however, the expression of its target *GALT9* was downregulated by 62% after 24 h of submergence. However, the expression of miR775 was significantly upregulated at 4 h but the expression of its target *GALT9* was not significantly changed. Furthermore, to analyse the tissue-specific expression, 7 dag shoot seedlings of *pMIR775A:GUS* and *pGALT9:GUS* transgenic plants were analysed at two time points, 4 h and 24 h, during submergence stress (Fig. 5B-G). Interestingly, we found similar results to those obtained using stem-loop qRT-PCR: under normoxic (normal level of oxygen) conditions, *pMIR775A:GUS* and *pGALT9:GUS* seedlings showed a basal level of expression in untreated seedlings (0 h). At 4 h after submergence, *Arabidopsis* seedlings had a mild elevation of *pMIR775A:GUS* expression; however, 24 h after submergence, *pMIR775A:GUS*

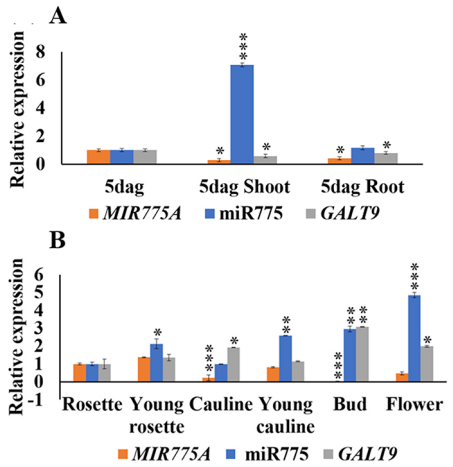

Fig. 4. Relative expression of *MIR775A*, miR775 and *GALT9* in various tissues of *Arabidopsis*. (A) 5 dag seedlings and (B) 35 dag plant. Data are mean±s.e.m. of three independent experiments. Asterisks indicate significant statistical differences (***$P\leq0.001$, **$P\leq0.01$ and *$P\leq0.05$, two-tailed Student's *t*-test).

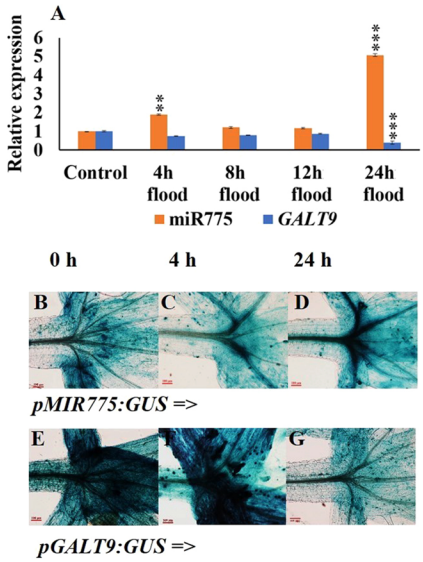

Fig. 5. Expression pattern of *MIR775A* and its target, *GALT9*, during submergence stress in *Arabidopsis* seedlings at different time points. (A) Relative expression levels of miR775 and *GALT9* during submergence stress at different time points. (B-D) Tissue-specific expression of *pMIR775A:GUS* in (B) 0 h (control), (C) 4 h and (D) 24 h. (E-G) Tissue-specific expression of target *pGALT9:GUS* at (E) 0 h (control), (F) 4 h and (G) 24 h. Data are mean±s.e.m. of three independent experiments. Asterisks indicate significant statistical differences (***$P\leq0.001$, and **$P\leq0.01$, two-tailed Student's *t*-test). *n*=10. Scale bars: 100 µm.

Development (2022) 149, dev199974. doi:10.1242/dev.199974

expression was upregulated (Fig. 5B-D), whereas expression of the *pGALT9:GUS* expression was significantly downregulated in shoot tissue (Fig. 5G). This result highlights the potential role of miR775 and its target *GALT9* during submergence stress in *Arabidopsis*.

Submergence recovery in miR775-Oe, *MIM775* and *galt9* plants

Complete submergence leads to the overproduction of different reactive oxygen species (ROS) due to the oxygen-deficient conditions (Bailey-Serres and Voesenek, 2008). Previously, we have shown that the expression of miR775 and *GALT9* was dynamically affected in a complementary way during submergence stress (Fig. 5). Therefore, we were interested to estimate the survival ability of different miR775 transgenic lines and of *galt9*. To estimate the survival rate, we treated different transgenic lines at the same stage (3 weeks old) (miR775-Oe1, miR775-Oe2, *galt9* and *MIM775-1*, *MIM775-2*) in complete submergence for 5 days, and estimated their survival rate after 5 days of desubmergence (5 DADS). We observed that nearly ∼75% of the wild-type (Col-0) plants survived during submergence recovery; however, the survivability rate was higher in miR775-Oe lines (∼85-90%) and *galt9* (∼90%). The survival rate of *MIM775* was reduced to ∼50%. (Fig. 6M). These results indicate that miR775-mediated regulation of its target gene *GALT9* contributes to the plant survival during post-submergence recovery.

Submergence stress altered the ROS levels in miR775-Oe, *MIM775* and *galt9* plants

To further understand the molecular function of the miR775-*GALT9* module during submergence stress in *Arabidopsis*, we analysed reactive oxygen species (ROS) accumulation. Hydrogen peroxide (H_2O_2) is one of the major ROS that accumulates during various abiotic and biotic stresses (Liu et al., 2010). We have estimated the ROS (here H_2O_2) level in different miR775 transgenic lines (miR775-Oe and *MIM775*) and in the *galt9* mutant in 12 dag seedlings after 5 days of submergence through DAB staining. The accumulation of H_2O_2 was highest in *MIM775-1* and *MIM775-2* (Fig. 7A-F). The level of H_2O_2 reduced in miR775-Oe1, miR775-Oe2 and *galt9*, when compared with Col-0 control (Fig. 7A-F). Furthermore, we quantified the ROS intensity by using ImageJ (https://imagej.nih.gov/ij/download.html) (Fig. 7G). Next, we quantified the accumulation of *RBOHD*, a core hypoxia marker gene, after the 5 days of desubmergence and we found increased expression of *RBOHD* in *MIM775-1* (2.19) but decreased expression of *RBOHD* in miR775-Oe1 (by 99%) and *galt9* (by 97%) (Fig. 7H). Increased expression of *RBOHD* in *MIM775* was persistent even after 5 DADS, suggesting ROS accumulation. This might have led to impaired growth during submergence due to the higher cell death. These higher levels of functional miR775, in miR775-Oe lines, promoted the plant survival ability during recovery from submergence stress, which might have reduced accumulation of ROS. Altered ROS levels in different miR775 transgenic and *galt9* lines suggest the differential ability of cells to survive.

Expression of senescence-associated genes (SAGs) and chlorophyll content were altered by post-submergence recovery

Our results showed the poor recovery in *MIM775* lines after submergence, in contrast to miR775-Oe and *galt9* lines (Fig. 6M). The *MIM775* transgenic lines have small rosette leaves; however, the miR775-Oe and *galt9* lines were phenotypically similar to the Col-0 control under normal growth and developmental conditions. *MIM775* transgenic lines exhibited enhanced senescence and a high degree of chlorosis after 5 DADS (Fig. 6). We observed a reduction in senescence and chlorosis in miR775-Oe and *galt9* transgenic lines, when compared with *MIM775*. To further quantify chlorophyll breakdown, we estimated the level of chlorophyll A,

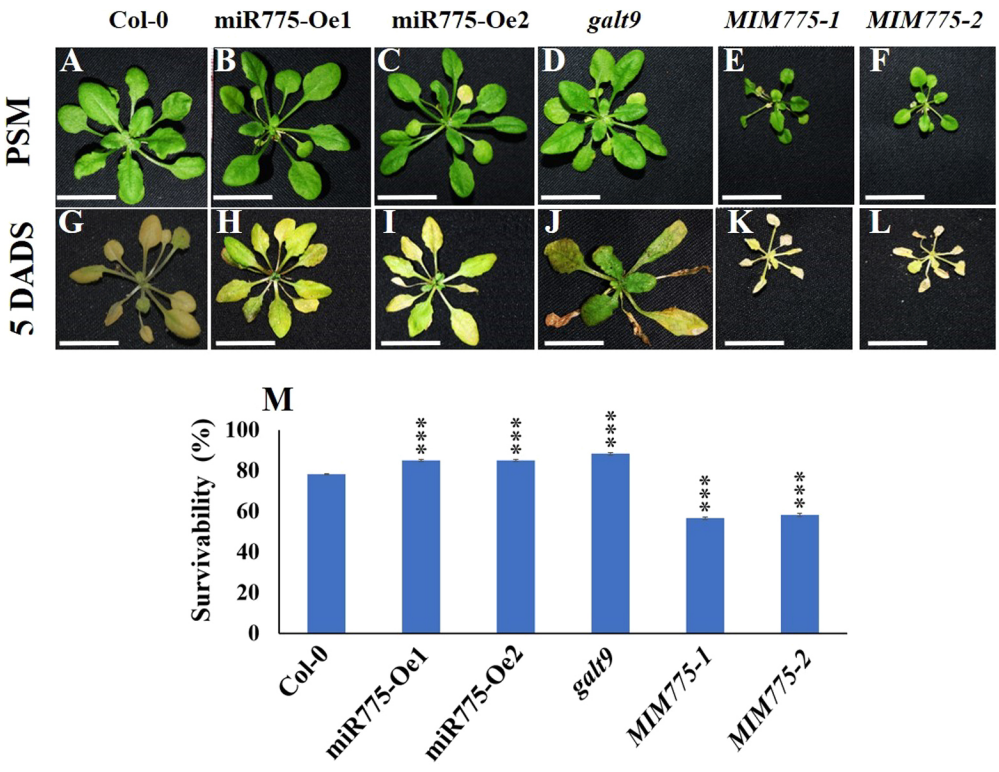

Fig. 6. Submergence recovery effect in *Arabidopsis* produced by miR775 and its target, *GALT9*. (A-F) Phenotypes of different transgenic lines in pre-submergence (PSM) conditions of (A) control (Col-0), (B,C) overexpression lines of miR775 (miR775-Oe1 and miR775-Oe2), (D) target mutant *galt9* and (E,F) target mimic lines of miR775 (*MIM775-1* and *MIM775-2*). (G-L) Phenotypes of different transgenic lines 5 days after de-submergence (DADS) of (G) Col-0, (H,I) overexpression lines of miR775 (miR775-Oe1 and miR775-Oe2), (J) target mutant *galt9* and (K,L) target mimic lines of miR775 (MIM*775-1* and *MIM775-2*). (M) Survivability (%) of different transgenic lines of miR775 along with control (Col-0) at 5 DADS. n=20. Data are mean±s.e.m. of three independent experiments. Asterisks indicate significant statistical differences (***P≤0.001, two-tailed Student's t-test). n=10. Scale bars: 2.5 cm.

Development (2022) 149, dev199974. doi:10.1242/dev.199974

chlorophyll B, total chlorophyll, carotenoids and xanthophylls at 5 DADS (Fig. 8A-D). We observed a reduction in total chlorophyll levels in the *MIM775* transgenic lines, in contrast to miR775-Oe and *galt9* transgenic lines. The level of chlorophyll A, chlorophyll B and xanthophyll was also reduced in *MIM775* lines (Fig. 8A-D).

An increase in ROS level and reduction in chlorophyll content after submergence stress is related to precocious senescence. Our results indicate that miR775-Oe and *galt9* plants survived through the submergence stress by reducing ROS levels and chlorosis, and, therefore, by delaying the senescence. On the other hand, the early senescence observed in *MIM775* plants (post-submergence) could be due to excessive ROS levels and reduced chlorophyll content (Fig. 7A-F,G; Fig. 8A-D).

Different abiotic and biotic stresses affect the expression of SAG genes such as *SAG12*, *SAG29* and *ORE1*, which further govern leaf senescence (Seo et al., 2011; Yeung et al., 2018; Bengoa Luoni et al., 2019; Ueda et al., 2020). We sought to determine whether miR775-*GALT9*-mediated post-submergence recovery and senescence, as evidenced by the phenotype in miR775 transgenic and *galt9* lines, involved SAG*s*. To address this, we compared the expression levels of *SAG12*, *SAG29* and *ORE1* during post-submergence recovery. The expression levels of *SAG12*, *SAG29* and *ORE1* was downregulated in miR775-Oe1 and *galt9* transgenic lines, whereas expression was upregulated in *MIM775-1* (Fig. 8E). These data suggest that the miR775-*GALT9* module regulates submergence tolerance and post-submergence recovery by modulating the expression of SAGs (*SAG12*, *SAG29* and *ORE1*) in *Arabidopsis*.

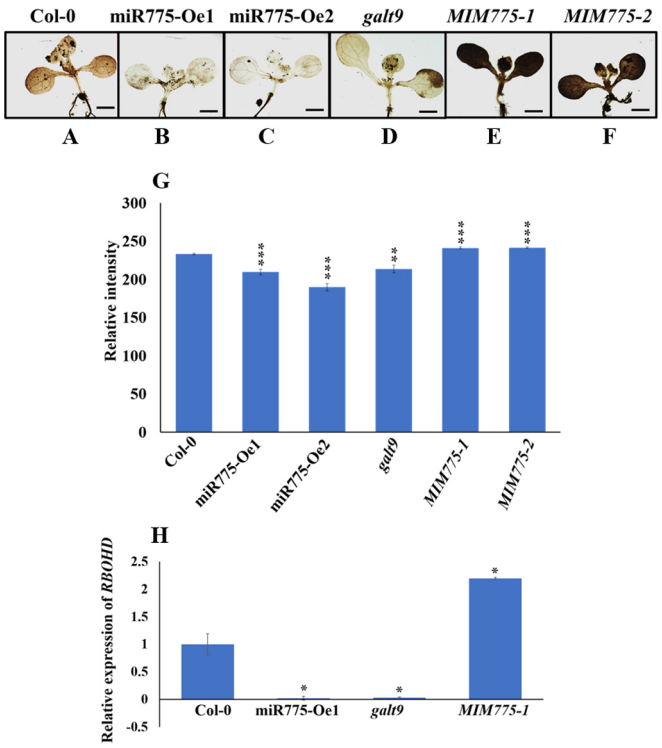

Fig. 7. Controlled ROS production is essential for recovery signalling. (A-F) Representative microscopic images of H_2O_2 accumulation (brown) in a 7 dag plant, 5 days after submergence. (A) Col-0, (B,C) overexpression lines of miR775 (miR775-Oe1 and miR775-Oe2), (D) target *galt9* and (E,F) target mimic lines of miR775 (*MIM775-1* and *MIM775-2*). (G) Quantification of ROS intensity using ImageJ software. (H) Relative mRNA abundance of *RBOHD* measured by qRT-PCR in Col-0, miR775-Oe1, *galt9* and *MIM775-1* in rosette leaves 5 days post-submergence. Data are mean±s.e.m. of three independent experiments. Asterisks indicate significant statistical differences (***$P \leq 0.001$, **$P \leq 0.01$ and *$P \leq 0.05$, two-tailed Student's *t*-test). *n*=20. Scale bars: 2 cm.

Putative molecular mechanisms and hormonal crosstalk during post-submergence recovery

Phytohormones, such as ethylene and ABA, promote leaf senescence (Wang et al., 2021). In *Arabidopsis*, ethylene promotes leaf senescence through a signalling cascade mediated by *ETHYLENE INSENSITIVE 2* (*EIN2*), *EIN3* and *ORE1* (Kim et al., 2009, 2014). EIN3, a pivotal TF of ethylene signalling directly activates the expression of *ORE1* and *SAG29* to promote leaf senescence (Kim et al., 2014; Qiu et al., 2015; Zhang et al., 2018). To confirm this further, we quantified the expression of *EIN2* and *EIN3*, which act upstream of *ORE1* and *SAG29*, and we found *EIN2* and *EIN3* upregulated by 2.65- and 22.39-fold, respectively, in *MIM775* (Fig. 8F). However, EIN2 and EIN3 were downregulated in miR775-Oe1 (by 92% and 79%) and in *galt9* (by 55% and 66%). It has been reported that senescence-associated NAM/ATAF1,2/CUC2 (NAC) TFs, such as ANAC019, ANAC047, ANAC055, ORE1 SISTER1 (ORS1) and ANAC102, and ANAC087, act downstream of *EIN2* and *EIN3*, respectively, to accelerate leaf senescence, chlorophyll breakdown and cell death, which ultimately inhibit post submergence recovery (Kim et al., 2014; Yeung et al., 2018).

It has been shown previously in the current study that the expression of *RBOHD*, a core hypoxia marker gene was increased in *MIM775-1* (2.19-fold) when compared with miR775-Oe1 and *galt9* lines, after 5 DADS (Fig. 7H). Increased expression of *RBOHD* in *MIM775* was persistent even after 5 DADS, suggesting ROS accumulation. It has been shown that osmotic stress causes oxidative stress, leading to oxidative cell damage, and expression of the ABA biosynthesis gene *NINE-CIS-EPOXYCAROTENOID DIOXYGENASE 3* (*NCED3*) is drastically upregulated by osmotic stress (Xiong et al., 2002; Tamang and Fukao, 2015). Furthermore, we quantified *NCED3* which has been shown to be upregulated by osmotic/oxidative stress and we found the expression of *NCED3* was upregulated by 5.84-fold in *MIM775-1* (Fig. 8F) compared with miR775-Oe1 and *galt9* (reduced by 89% and 90%, respectively). This increased *NCED3* leads to accumulation of ABA and thus promotes stomatal closure, which inhibits dehydration and ultimately affects post-submergence recovery. These data suggest that the miR775-*GALT9*-ET-ABA module regulates post-submergence recovery by modulating ethylene signalling and ABA biosynthesis in *Arabidopsis*.

DISCUSSION

The miRNA-mediated gene regulation is crucial for the plant growth, development and physiological responses, which facilitated the origin and evolution of miRNA through positive selection. Many of the miRNAs are evolutionarily categorized as ancient or young, based on their origin in plant species (Zhang et al., 2006; Voinnet, 2009). Similarly, miR775 appears to be a so-called young miRNA, which is due to its species-specific presence in *Arabidopsis* (Lu et al., 2006; Rajagopalan et al., 2006). Earlier studies reported that plant species from *Poaceae* and *Brassicaceae* possessed many species-specific non-conserved miRNAs that originated through rapid spontaneous evolution (Zhang et al., 2006; Cui et al., 2017). Our study shows the *de novo* origin of *MIR775A* in *Arabidopsis*. The genomic location of *MIR775A* and its validated target *GALT9*, and higher conservation of miR775-binding site at *GALT9* does not support the canonical modes of origin and evolution of miR775 (Fig. 1). Furthermore, we found its gene structure acquired through the acquisition of TSS and TATA-box upstream of two consecutive

Development (2022) 149, dev199974. doi:10.1242/dev.199974

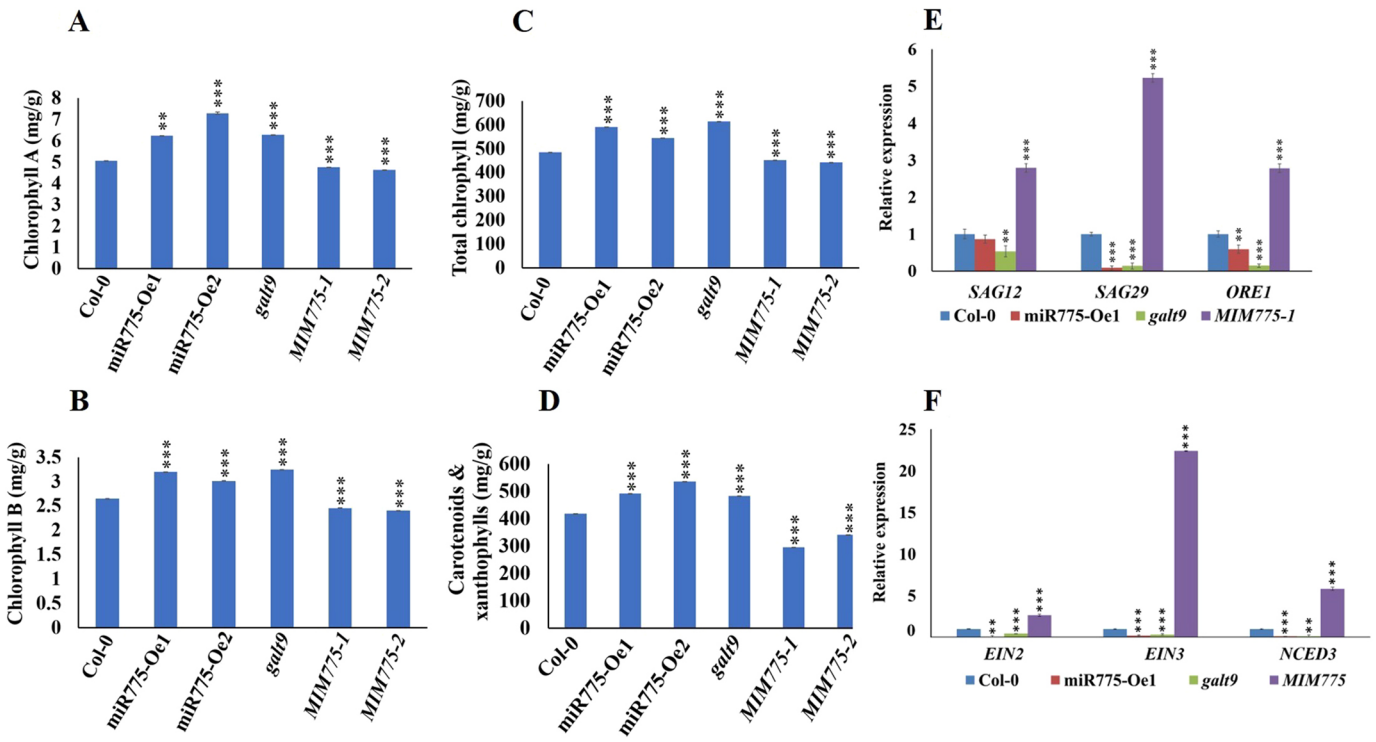

Fig. 8. Effect of submergence on chlorophyll content and expression of senescence-associated genes (SAGs). (A-D) Estimations of chlorophyll A, chlorophyll B, total chlorophyll, and carotenoids and xanthophylls, respectively, in control Col-0, in overexpressing lines (miR775-Oe1 and miR775-Oe2), in *galt9*, and in *MIM775-1* and *MIM775-2* 5 days after de-submergence (DADS). (E,F) Relative expression levels of senescence-associated gene (SAGs) *SAG12*, *SAG29* and *ORE1* (E) and *EIN2*, *EIN3* and *NCED3* (F) and in control Col-0, in an overexpressing line of miR775 (miR775-Oe1), in a mutant of target *galt9* (*galt9*) and in a target mimic line of miR775 (*MIM775-1*) at 5 DADS. Data are mean±s.e.m. of two independent experiments for chlorophyll estimation and three independent experiments for relative expression of qRT-PCR. Asterisks indicate significant statistical differences (***$P \leq 0.001$ and **$P \leq 0.01$, two-tailed Student's *t*-test).

genes, *snoRNA* and *MIR775A* dicistronic in nature (Qu et al., 2015) (Fig. 1A, Fig. S1A). The continuous preferential selection pressure might be acted upon by the *Arabidopsis* genome for the acquisition of promoter elements to regulate target gene *GALT9*. However, genetic drift, due to lack of selection, might have resulted in the loss of these genes in subsequent species divergence (Voinnet, 2009).

Identification of miRNA, target genes and their conservation across the species reveals the role of miRNA-target gene modulation in various aspects of plant growth and their physiology. Techniques such as degradome PARE analysis often enables the identification of conserved and novel targets. Our degradome analysis suggested *GALT9* was a strong target of miR775 in *Arabidopsis* (Fig. 1C). Consistent with other observations, *GALT9* is validated and established as a bona fide target of miR775 (Fig. 1C) (Fahlgren et al., 2007; Mishra et al., 2021; Zhang et al., 2021). Interestingly, however, variations in the cleavage site of miR775 were obvious (Fig. 1C), which might depend upon the stage of growth and growth condition, and be due to the biogenesis of miR775 from the 3′ end of its stem-loop precursor (Fig. 1B). Additionally, in the present study, we validated our *in silico*-based prediction using I-TASSER and AtSubP to show that GALT9 protein localizes in the Golgi body (Figs S4-S5). The role of GALT9 was deduced from the predicted protein 3D structure through I-TASSER, which shows its protein glycosylation activity, as a part of post-translational modifications (PTM) required for folding and stabilizing the translated protein structures.

Environmental factors or abiotic stresses are known to influence the expression of many miRNAs that are involved during the regulation of physiology, as well as during growth and development of plants. It has been reported previously that the hypoxic condition, caused by flood or high altitude, leads to the induction of miR775, indicating its potential role in hypoxia-inducing stresses (Moldovan et al., 2010; Liu et al., 2012; Tripathi et al., 2019).

Submergence severely affects plant growth, development, survivability and yield by reducing light availability and stomatal opening, and therefore gaseous exchanges, which ultimately affects photosynthesis and respiration. So efficient recovery from the submergence stress is vital for plant growth and survival. In the current study, we show the complementary regulation of the miR775-*GALT9* module during the submergence stress-induced senescence and post-submergence recovery.

Our results indicate the dynamic spatio-temporal expression pattern of miR775 and its target *GALT9* through reporter lines of *pMIR775A:GUS* and *pGALT9:GUS* under normal and submergence stress (Figs 3 and 5). Under normal conditions (without submergence), all the miR775 transgenic lines and *galt9* mutants were green and healthy; however, leaves of *MIM775* lines were small in size (Fig. 6A-F). Mutation in the light-response/signalling gene *HY5* is known to affect plant organ or leaf size (Zhang et al., 2021). We showed that the expression of miR775 was increased in the shoot of the *hy5-1* mutant (Fig. S6B). Furthermore, HY5 protein is directly bound to the promoter of *MIR775A*, as shown by the yeast-one-hybrid experiment (Fig. S6A). Therefore, HY5-mediated regulation of miR775 contributes to the altered leaf shape (organ size) (Fig. S7). These results implicate HY5 in miR775-*GALT9*-mediated organ size regulation (Zhang et al., 2021). Many *GALT9* colocalized genes that encode Golgi body localized proteins (such as ACLA1, CGR2 and CGR3; Table S4)

Development (2022) 149, dev199974. doi:10.1242/dev.199974

have previously been shown to play a key role in plant development, such as *ATP-CITRATE LYASE A-1* (*acla1*) and *COTTON GOLGI-RELATED 2* (*cgr2-1* and *cgr3-1*), the mutants of which have relatively smaller organ size (Fatland et al., 2005; Kim et al., 2015b).

We have characterized the miR775-*GALT9* module for its role in submergence stress recovery. Submergence stress causes reduction in oxygen level (hypoxia) (Nishiuchi et al., 2012; Ahmed et al., 2013; Chen et al., 2015; Yeung et al., 2018; Loreti and Striker, 2020; Nakamura and Noguchi, 2020). In our results, transgenics [miR775 overexpression (miR775-Oe1) and target mimic of miR775 (*MIM775*)] and obtained *galt9* mutant lines revealed significant differences in their submergence stress tolerance and post-submergence recovery. Among these miR775 transgenic and mutant lines, miR775-Oe1 and *galt9* exhibited the reduced accumulation of ROS (Fig. 7A-F,G). However, the *MIM775-1* line displayed an increased accumulation of ROS. It has been previously reported that after desubmergence, the reillumination conditions lead to the production of ROS in recovering tissues (Elstner and Osswald, 1994; Smirnoff, 1995). ROS production differed between the miR775-Oe1, *galt9* and *MIM775* lines, which corresponded to higher *RBOHD* accumulation during recovery in *MIM775*. *RBOHD*, a key hypoxia gene, and the *RBOHD*-mediated ROS burst are crucial for submergence tolerance and recovery (Yeung et al., 2018). Balanced ROS production is crucial and needs to be countered by an effective antioxidant mechanism that can control excessive ROS production and associated damage in *Arabidopsis*. However, the recovery signals regulating *RBOHD* remain to be determined. A recent report shows that ABA and ethylene responses in *Arabidopsis* are crucial for submergence tolerance and recovery (Yeung et al., 2018). Increased cell death in *MIM775-1* during submergence stress is also evident in the shoot after desubmergence (Fig. 7A-F,G). Upregulation of SAG genes, including *ORE1*, *SAG12* and *SAG29*, is marked during senescence (Weaver et al., 1998; Seo et al., 2011; Kim et al., 2014; Qiu et al., 2015; Ding et al., 2016; Yeung et al., 2018; Ueda et al., 2020). Our results show higher upregulation of *EIN2*, *EIN3*, *ORE1*, *SAG12* and *SAG29* in *MIM775* lines, in comparison with miR775-Oe1, *galt9* and Col-0 (Fig. 8E).

The miR775-Oe1 and *galt9* transgenics lines were healthy in comparison with Col-0 and *MIM775-1* at 5 DADS (Fig. 6A-L). *MIM775* lines were poorly affected by the submergence-induced stress and showed early senescence during the submergence (Fig. 6M) (Qiu et al., 2015; Yeung et al., 2018). Submergence stress led to the yellowing of leaves in *MIM775-1* lines where chlorophyll content was lowest, in comparison with miR775-Oe1 and *galt9* (Fig. 8A-D), suggesting that the miR775- *GALT9* module regulates senescence and post-submergence recovery (Fig. 8A-D).

Ethylene is known to be a senescence-accelerating hormone and its signalling involves the *ETHYLENE–INSENSITIVE 2* (EIN2), EIN3 and NAC TFs to regulate leaf senescence and chlorophyll degradation in *Arabidopsis* (Neljubow, 1901; Crocker, 1932; Kim et al., 2015a; Iqbal et al., 2017). EIN3 directly activates the master regulators of SAG genes, *ORE1* and *SAG29*, to promote leaf senescence (Wang et al., 2021).

EIN2 mediates leaf senescence by transducing ANAC019, ANAC047, ANAC055 and ORS1 TFs via an EIN3-independent pathway. However, ANAC087 and ANAC102 TFs were preferentially activated by *ORE1* to promote leaf senescence, chlorophyll degradation and cell death (Kim et al., 2014). Phytohormone ABA and ethylene regulate dehydration and senescence during submergence recovery by modulating SAG genes and *ORE1* (Yeung et al., 2018). Enhanced expression of *RBOHD* promotes ROS accumulation, which ultimately accelerates the expression of *NCED3* by oxidative stress (Xiong et al., 2002). The ABA accumulation inhibits dehydration by stomatal closure and hampers post-submergence recovery (Xiong et al., 2002; Yeung et al., 2018).

The role of GALT9 is deduced from the modelled protein structure using I-TASSER, which reveals its protein glycosylation activity, which is a part of the post-translational modifications (PTM) required for folding and stabilizing the translated proteins [e.g. many membrane proteins, secreted proteins and vacuolar proteins (Schwarz and Aebi, 2011; von Schaewen et al., 2008)]. Earlier studies have shown that the hampered maturation of *N*-glycan in Golgi complexes reduces the stress tolerance ability (Kang et al., 2008; Nagashima et al., 2018). Some of the proteins (EIN2 and RBOHD, etc.) involved in the post-submergence-directed senescence network, were membrane bounded and acted as signal receptors. However, any perturbation in *N*-glycosylation disrupts the activity of membrane-bounded signal receptors (Nagashima et al., 2018). Furthermore, we observed that *SAG12*, a senescence-associated vacuolar protein, undergoes *N*-glycosylation (https://www.uniprot.org/uniprot/Q9FJ47#ptm_processing) and might be processed by GALT9 (Figs S4 and S5).The connection between the miR775-*GALT9* module and ethylene and ABA pathways is likely to be indirect. Given that GALT9 is not a transcription factor, it is likely to regulate the downstream genes through post-translational modification. N-linked glycosylation of phytohormonal pathway components (proteins) is crucial for hormonal homeostasis, and is required for physiological and developmental responses (Jiao et al., 2020; Li and Lan, 2017; Ostrowski and Jakubowska, 2014). Recently, it was predicted that ethylene biosynthetic pathway genes, such as S-adenosyl-l-methionine (SAM), aminocyclopropane-1-carboxylic acid synthase (ACS) and ACC oxidase (ACO) proteins have N-linked glycosylation sites (Ahmadizadeh et al., 2020). Ethylene is known to promote the accumulation of EIN2 and EIN3 (Qiao et al., 2009), which showed enhanced expression in *MIM775* lines (Fig. 8F), which have higher *GALT9* levels. Therefore, we hypothesized that GALT9 mediated possible N-glycosylation of ethylene biosynthetic component (e.g. SAM, ACS and ACO) might have led to the altered accumulation of EIN2 and EIN3, which have affected post-submergence recovery in mutants/transgenics of miR775/*GALT9* (Figs 8F and 9). On the other hand, the accumulation and homeostasis of endogenous ABA levels is regulated by AtBG1 (an efficient β-glucosidase), which is involved in the hydrolysis of glucose-conjugated ABA (Jin et al., 2011; Lee et al., 2006). As the glycoprotein AtBG1 possessed N-glycosylation sites, it is possible that GALT9-mediated glycosylation helps in the activation of AtBG1, which in turn hydrolyses the conjugated form of ABA (glucose-ABA) to produce active ABA. ABA increases the expression of *NCED3* (an ABA biosynthetic gene) in a positive-feedback mechanism (Barrero et al., 2006). We show the increased expression of *NCED3* in *MIM775* lines during post submergence recovery, which might be due to GALT9-mediated glycosylation of AtBG1 (Figs 8F and 9).

In summary, we illustrate the role of the miR775-*GALT9* module during submergence-induced recovery response. Our results suggest that miR775 promotes recovery after submergence by downregulating the expression of target *GALT9*. *GALT9* overexpression, produced in the *MIM775* line, led to the severe senescence of plants (Fig. 6). The miR775-*GALT9* module regulates the post-submergence recovery through the regulation of *EIN2*, *EIN3* and SAGs either directly or indirectly. Increased expression of *EIN2*, *EIN3*, *NCED3* and SAGs in the *MIM775* lines promotes cell death and chlorosis, which may be the consequence of

Development (2022) 149, dev199974. doi:10.1242/dev.199974

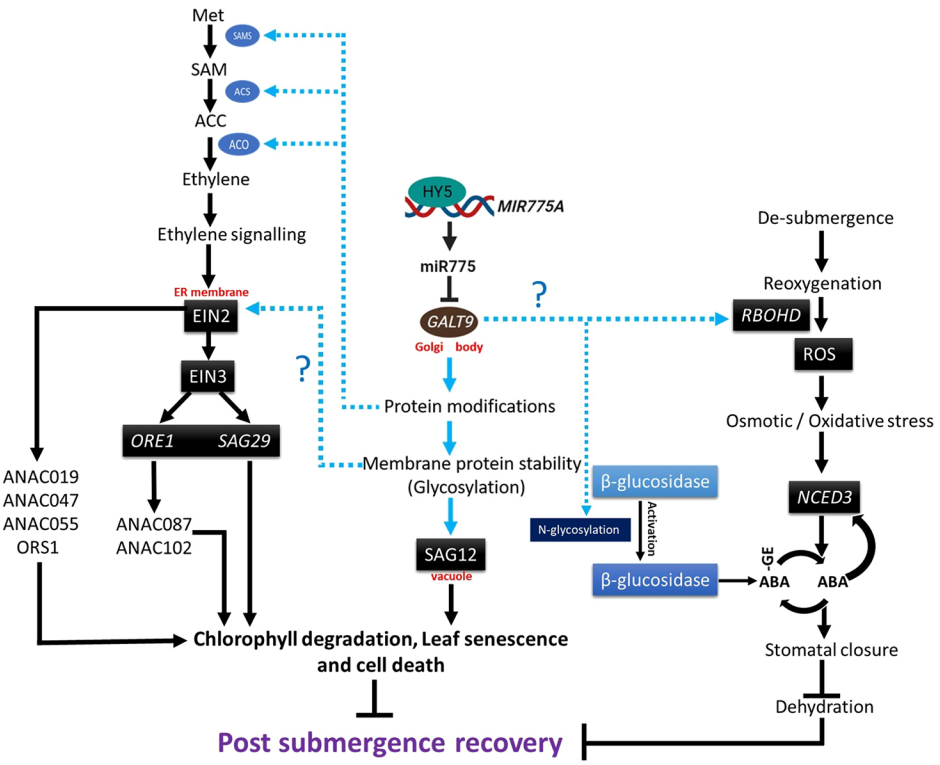

Fig. 9. Model showing the signalling network mediating post-submergence recovery in *Arabidopsis*. The expression of genes changed in our study are highlighted in black boxes. The solid blue lines indicate the possible protein glycosylation through GALT9 during post-submergence recovery. The blue ovals show the possible role of GALT9 in N-linked glycosylation of SAM, ACS and ACO proteins. The N-linked glycosylation of β-glucosidase produces active β-glucosidase (blue rectangles), which catalyses hydrolysis of glucose-conjugated ABA to produce active ABA. Blue dotted lines show the putative role of GALT9, either direct or indirect, in the regulation of downstream genes/proteins. GALT9 promotes the expression of EIN2, and thereby expression of downstream EIN3, ORE1 and SAG29. EIN2 is known to promote chlorophyll degradation, leaf senescence and cell death via ANAC019, ANAC047, ANAC055 and ORS1, whereas *ORE1* does the same via ANAC087 and ANAC102 (Kim et al., 2014). GALT9, by an unknown mechanism, induces the expression of *RBOHD*, which promotes ROS and induces ABA production through induced expression of *NCED3*, and thus affects post-submergence recovery.

increased ROS due to altered *GALT9* abundance and changes in the ethylene and ABA biosynthesis pathway genes (Fig. 8E). Based on our findings, we proposed a hypothetical model showing the importance of miR775-*GALT9* module in regulating the post-submergence recovery process in *Arabidopsis* (Fig. 9).

MATERIALS AND METHODS

Evolutionary analysis of miR775 in *Arabidopsis*

We evaluated the mode of origin of miR775 in *Arabidopsis*. We calculated the distance between *MIR775A* (Chr1:29422452) and *GALT9* (Chr1:19873727) genes and found to be 9.55 Mbp apart on chromosome 1 (Araport11). Furthermore, sequence alignment between *GALT9* and *MIR775A* did not show any duplication of *GALT9* in *MIR775A*. Consequently, we also searched for conservation or variation of complementary miR775-binding sites in *GALT9* homologs through multiple sequence alignment using ClustalX (Larkin et al., 2007). Multiple sequence alignment of the top 19 hits of the *GALT9* homologs have shown conserved complementary miR775-binding sites (Fig. S1b). Furthermore, we predicted the promoter of *MIR775A* using the tool TSSPlant (http://www.softberry.com/cgi-bin/programs/promoter/tssplant.pl). Upstream of *MIR775A*, we found *snoRNA* (AT1G09787.1) at a distance of 92 bp, but no transcription start site (TSS) or TATA box. Therefore, we took the upstream sequence extended from *MIR775A* to AT1G78200, and predicted the TATA box and TSS using TSSPlant at distance of 387 bp and 356 bp, respectively, upstream of *MIR775A*.

Validation of the miR775 target using degradome data

We analysed the target of miR775 through the analysis of *Arabidopsis* degradome PARE data available at Sequence Read Archive (SRA) in NCBI (SRR3143654–11-day-old seedling, SRR7093799 – leaf sample of stage 5) using the tool CleaveLand v4.5 (used to find evidence of sliced targets of small RNAs from degradome data) (Addo-Quaye et al., 2009). We retrieved SRA datasets SRR3143654 and SRR7093799, and then further converted these into fastq and, subsequently, into fasta file formats using locally installed tools fastq-dump from SRA Toolkit (https://www.ncbi.nlm.nih.gov/books/NBK158900/) and FASTX-Toolkit (http://hannonlab.cshl.edu/fastx_toolkit/), respectively. The tool fastx_trimmer from FASTX-Toolkit was used for trimming the adapter sequences from these datasets. Furthermore, the mature miR775 sequence was used as a query to search against the whole-genome cDNA sequences of *Arabidopsis* (https://www.arabidopsis.org/download/index-auto.jsp?dir=%2Fdownload_files%2FSequences%2FAraport11_blastsets). The SRA datasets, mature miR775 sequences and cDNA reference sequences of *Arabidopsis* were used for the analysis of the miR775 target through the CleaveLand4 pipeline using default settings. The aligned reads of SRA datasets were considered as targets that were being cut at the 10th position in miR775. The miRNA-target cleavage site that has CleaveLand analysis category (0-4) ≤2, lowest Allen et al. (2004) score (0-∞), and highest MFE ratio (0-1) were considered as the best target.

Construction of transgenic lines

For miR775 overexpression, the DNA fragments corresponding to the precursors of 238 bp were cloned, fused to the cauliflower mosaic virus 2X35S promoter gateway cloning vector pMDC32 and transformed into ecotype Columbia (Col-0). For the expression pattern of *pGALT9:GUS*, the 1256 bp length of promoter sequence of *GALT9* was cloned into pCAMBIA1301, fused to the glucuronidase (GUS) reporter gene as *pGALT9:GUS* and transformed into Col-0 via *Agrobacterium*-mediated transformation. For localization and target validation, the full-length CDS of *GALT9* (1038 bp) was cloned in the pCAMBIA1304 vector frame in the same way as *35S:GALT9:GFP*, by removing the stop codon. The target mimic line *MIM775* was generated by modifying the *IPS1* gene (Todesco et al., 2010). *MIM775* target mimic constructs were placed in pGREEN vectors under the constitutive CaMV 35S promoter, which is resistant against BASTA. Col-0 ecotype was used as a control throughout the experiment. Seeds of *galt9* (AT1G53290) SALK_015338 were obtained from *Arabidopsis* Biological Resource Center (ABRC) (Ohio State University). The two independent lines showing the maximum upregulation of miR775, miR775-Oe1 (14.19-fold) and miR775-Oe2 (5.46-fold) were selected on hygromycin B for further analysis in theT3 generation. For miR775 mimic (*MIM775*) lines, the two lines exhibiting the maximum upregulation of *GALT9* in *MIM775-1* (3.98-fold) and *MIM775-2*

Development (2022) 149, dev199974. doi:10.1242/dev.199974

(2.55-fold) were selected on BASTA for the further analysis in the T3 generation. Additionally, we generated *GALT9*-Oe1 (2.44-fold) and *GALT9*-Oe2 (3.04-fold), and selected on hygromycin B for further analysis in the T3 generation. Primer details are provided in Table S3.

Plant growth and submergence treatment

For all the experiments, the *Arabidopsis* seeds were first sterilized by seed wash buffer [70% ethanol and 0.1% (v/v) Triton X-100] and then germinated on half-strength Murashige and Skoog (½MS) medium (HiMedia) supplemented with 1% sucrose and 0.8% agar (Murashige and Skoog, 1962). The plants were grown vertically in a controlled environment at 21-22°C, under the 16 h light:8 h dark cycle of white light intensity at 120 µmol m^{-2} s^{-1}. The above experiments were repeated in triplicates to ensure precision and reproducibility.

For submergence treatment, we used a 3-week-old Col-0 plant. The disinfected containers were filled with Milli-Q water overnight before the treatment to maintain temperature equilibrium (21-22°C), as previously described with some modifications (Yeung et al., 2018), and submerged (8 h after the start of the photoperiod) in ∼6 cm water depth in a dark, humidity-controlled room (Yeung et al., 2018). After 5 days of submergence, de-submerged plants were returned to normal growth conditions for 5 days to follow the post-submergence recovery. Submergence-related experiments were performed at 2:00 PM (8 h after the start of the photoperiod).

Conditions for the expression analysis of *MIR775A* and its target *GALT9* during submergence stress in *Arabidopsis* seedlings at different time points

For submergence treatment, the disinfected containers were filled with Milli-Q water overnight before the treatment to maintain the temperature equilibrium (21-22°C). The 7 dag seedlings of *pMIR7775A: GUS*, *pGALT9: GUS* and Col-0 plants were grown in square Petri plates containing ½ MS media (120×120×17 mm; Praveen Scientific Corporation, India). The plants were submerged (8 h after the start of the photoperiod) at 2:00 PM in ∼6 cm water depth in a dark, humidity-controlled room. The samples were harvested for GUS analysis at early and late time points of 4 h and 24 h. For control plants, the samples were kept in the dark for the same period without being submerged to rule out the effect of the dark on the results. Samples were then harvested for GUS analysis. For GUS analysis, samples were incubated at 37°C for 14.5 h.

Agrobacterium infiltration with transgenic constructs for validation of miRNA target

Four-week-old *Nicotiana benthamiana* leaves were used for target validation. miR775-Oe and miR839-Oe cloned in the pSITE-4NB vector and sensitive 35S:*GALT9:GFP* constructs were used for transformations in the *Agrobacterium tumefaciens* GV3101 strain. For infiltrations, the overnight cultures of individual constructs were harvested and then suspended in an infiltration buffer [pH 5.7, 0.5% glucose 10 mM $MgCl_2$, 150 µM acetosyringone and 10 mM 2-(N-morpholino) ethanesulfonic acid (MES)] and incubated at room temperature for 6 h. For target validation, *Nicotiana* leaves were infiltrated by 1 ml syringe with the target constructs (sensitive 35S:*GALT9:GFP*) alone or with EV+*35S:GALT9:GFP*, *35S:MIR775A+35S:GALT9:GFP* and *35S:MIR839A+35S:GALT9:GFP* in a 1:1 ratio. The plants were kept in a growth chamber maintained at 26°C (±2) and light intensity of 250 µmol m^{-2} s^{-1} and harvested after 48 h for RNA extraction. For target validation, the *HPTII* gene in the vector was used to normalize target abundance in qRT-PCR experiments. For precursor efficiency in qRT-PCR assays, the Ct value of precursor expression was checked to confirm the synthesis of precursor miRNA in the overexpression construct.

A homology search for miR775 and target *GALT9*

We performed BLAST for the identification of precursor *MIR775A* and *GALT9* homologs in other plants. We did not find any homolog of miR775 in plants, even by changing the search parameters of BLAST. However, *GALT9* shows homologs in other plants. A phylogenetic tree was reconstructed using the BLAST hits of *GALT9* through NCBI with the identity and query coverage (https://blast.ncbi.nlm.nih.gov/Blast.cgi).

3D structure prediction and analysis

The functional annotation of GALT9 protein was accomplished by analysing its 3D structure. However, a 3D solved structure of GALT9 is not present in the Protein Data Bank archive (PDB; https://www.rcsb.org/). Therefore, we used I-TASSER (Iterative Threading ASSEmbly Refinement), an online server (https://zhanglab.dcmb.med.umich.edu/I-TASSER/), for protein 3D structure prediction and structure-based function annotation, which use a hierarchical and multiple threading approaches. The 3D structures of the best predicted model of GALT9 were visualized using Chimera v1.6.2 (Fig. S3A). The stereochemical quality check through Ramachandran plot of the predicted GALT9 structure confirmed its stable structure (Fig. S3B). Simultaneously, the functional annotation was also predicted based on assigned enzyme commission (EC) numbers, gene ontology (GO) terms and ligand-binding sites with binding affinity (Zhang, 2008; Roy et al., 2010; Yang et al., 2015).

GALT9 protein and its subcellular localization *in planta*

To explore subcellular localization of GALT9 protein, we used an *Arabidopsis* Subcellular Localization Prediction Server (AtSubP, http://bioinfo3.noble.org/AtSubP/index.php). For the prediction of GALT9 subcellular localization, the amino acid composition-based Support Vector Machine (SVM) found that GALT9 is a Golgi apparatus protein. To validate the subcellular localization, the coding sequence of the *GALT9* gene (without the stop codon) was cloned into the pCAMBIA1304. The *35S:GALT9:GFP* construct was then transformed into the *Agrobacterium* tumefaciens GV3101 strain. *Agrobacterium* containing the *35S:GALT9:GFP* or *GmManI*-pBIN2 Golgi apparatus mCherry marker constructs were grown to saturation in Luria-Bertani (LB) medium. Cultures were centrifuged and resuspended in 10 mM $MgCl_2$, 10 mM MES and 150 mM acetosyringone, and kept at room temperature for 2 h. The cultures were then diluted to one OD600 unit and co-infiltrated into the abaxial side of young tobacco (*Nicotiana benthamiana*) leaf epidermis (4-week-old seedlings grown at 22°C) using a 1 ml syringe without the needle. Transformed leaves were analysed 72 h after infection of the lower epidermis. Subsequently, fluorescence microscopy was performed on a Nikon 80i to record and process the digital images. At least three independently transformed leaves were analysed.

Histochemical detection of GUS assay and microscopy

Histochemical GUS analysis was carried out by putting the samples into appropriate amounts of GUS histochemical buffer [50 mM sodium phosphate (pH 5.7), 50 mM EDTA (pH 8.0), 0.1% Triton X-100, 2 mM potassium ferrocyanide, 2 mM potassium ferricyanide and 1 mM 5-bromo-4-chloro-3-indolyl-β-D-glucuronic acid (X-Gluc)] and incubated at 37°C for 14.5 h. Stained samples were washed with a de-staining solution of ethanol:acetone:glycerol (3:1:1, v/v/v) to remove chlorophyll and then, after incubating the samples in chloral hydrate (TCI Chemicals) for 1 h, microscopy was performed using a Nikon80i and an Olympus SZX16 to record and process the digital images.

Total RNA extraction and quantitative real-time PCR

Gene-specific primers were designed using Integrated DNA Technologies software and custom synthesized by Sigma Aldrich. The total RNA was extracted by using TRIzol (TRI reagent). Purified RNA used for single-stranded cDNA was synthesized from 2.5 µg RNA using an oligo (dT) primer using a high-capacity cDNA reverse transcription kit (Thermo Fisher Scientific). The RT reaction consisted of total RNA, 0.8 µl of 100 mM dNTP mix, 4 µl of 5× reaction buffer, 1 µl of random hexamer primer, 1 µl of oligodT and 1 µl of Revert aid RT enzyme in a final volume of 20 µl. The reaction was carried out at 25°C for 10 min and 37°C for 2 h followed by denaturation at 85°C for 5 min. For performing qRT-PCR, the cDNAs were diluted to 20 ng with sterile MilliQ water. For each tissue type, separate PCR amplification reactions were set up for detecting

Development (2022) 149, dev199974. doi:10.1242/dev.199974

different genes. The qRT-PCR reaction was set up by mixing 5 µl of 2× PowerUp SYBR Green PCR Master Mix (Applied Biosystems), 0.5 µl of 10 µM each of forward and reverse primers, 2 µl (40 ng) of cDNA and sterile MilliQ water to adjust the reaction volume to 10 µl. qRT-PCR was carried out in an Applied Biosystems ViiA 7 Real-Time PCR System with PowerUp SYBR Green Master Mix. The relative transcript level was calculated by using the $2^{-\Delta\Delta CT}$ method, which was normalized to *ACTIN7* as previously described (Wang et al., 2014; Singh et al., 2020b).

For stem-loop cDNA synthesis, a total of 200 ng of purified RNA was taken then mixed with 0.5 µl 10 mM dNTP and nuclease-free water. The mixture was incubated at 65°C for 5 min, kept on ice for 2 min, briefly centrifuged and added with 4 µl of 5× Reaction buffer (Thermo Fisher Scientific), 2 µl of 0.1 M DTT, 0.25 µl of RiboLock RNase Inhibitor (stock: 20 units/µl), 0.25 µl of RevertAid H Minus M-MuLV Reverse Transcriptase (stock: 200 units/µl), and 1 µl of stem-loop primer (stock: 1 µM) to make a final reaction volume of 20 µl. After gentle mixing, a centrifuge was used to bring the solution to the bottom of the tube and cDNA synthesis was performed as previously described (Varkonyi-Gasic et al., 2007). The cDNA was diluted up to two times before performing the real-time PCR. Fold change was calculated using the formula $FC=2^{-\Delta\Delta Ct}$ as previously described (Singh et al., 2017, 2020b; Gautam et al., 2020).

Histochemical detection of H_2O_2

The H_2O_2 staining agent 3,3′diaminobenzidine (DAB) (SRL), was dissolved in H_2O by adjusting the pH to 3.8 with KOH. Freshly prepared DAB solution was used to avoid auto-oxidation. The 7 dag seedlings were transferred for 5 days for submergence; after 5 days of submergence the seedlings were exposed to 1 h of normal conditions and then transferred for treatment by immersion and infiltration under vacuum with 1.25 mg ml^{-1} DAB staining solution for 15 min followed by incubation at room temperature for 6 h. The stained seedlings were then bleached out in ethanol:acetic acid:glycerol (3:1:1, v/v/v) solution for 30 min and then images were captured using an Olympus SZX16 microscope. ImageJ system software (https://imagej.nih.gov/ij/download.html) was used for the quantification of ROS intensity. The brown colour visualization of H_2O_2 was due to DAB polymerization.

Chlorophylls and xanthophyll's estimation

Chlorophyll and xanthophyll were extracted from 100 mg of rosettes leave with 96% (v/v) by DMSO dark incubation at 65°C for 30 min and cooled to room temperature for 15 min (Hiscox and Israelstam, 1979; Richardson et al., 2002). The absorbance (A) at 470, 645 and 663 nm by calibrating to zero with pure DMSO was measured using a spectrophotometer plate reader (Synergy HT Multi-Detection Microplate Reader, BioTek Instruments). Measurements were carried out in two biological replicates. Chlorophyll A and B concentrations (ChlA and ChlB) were calculated using the following Arnon's equations:

$$\text{Chlorophyll A(mg/g fresh weight)} = [(12.7 \times A663) - (2.69 \times A645)] \times (V/1000 \times W),$$

$$\text{Chlorophyll B(mg/g fresh weight)} = [(22.9 \times A645) - (4.68 \times A663)] \times (V/1000 \times W),$$

$$\text{Total chlorophyll content} = (2008 \times A645 + 802 \times A663) \times (V/1000 \times W)$$

and

$$\text{Carotenoids + xanthophylls(mg/g fresh weight)} = (1000 \times A470 - 1.90ChlA - 63.14ChlB/214) \times (V/1000 \times W),$$

where V=volume of extract (ml) and W=fresh weight of the sample (g).

Yeast one hybrid assays

Yeast one-hybrid assays (Y1Hs) were performed to verify the gene-gene interactions, using the Matchmaker Gold Y1H Library Screening System. The full-length CDS of *HY5* was subcloned into the pGADT7 AD vector and the promoter of *pMIR775A* (~152 bp) was constructed into the public vector according to the ClonExpress II One-Step Cloning Kit. Auto-activation and then interaction analyses were performed.

Determination of auto-activation concentration of AbA

A healthy colony was picked from the bait strains. The colony was resuspended in SD-Ura broth. The dilution was adjusted to 0.1, 0.01, 0.001 and 0.0001, and 10 µl of the culture was patched on the following media: (1) SD/-Ura with AbA (150 ng/ml), (2) SD/-Ura with AbA (250 ng/ml) and (3) SD/-Ura with AbA (500 ng/ml). Vector and construct details are as follows: (1) pGADT7 (for cloning of prey), (2) pAbAi (for cloning of bait), (3) pGADT7-Rec-p53/p53-AbAi (positive control) and (4) pGADT7 transformed in Y1H gold cells (negative control). Colonies were grown for 2-3 days at 28°C on SD/-Ura plates.

Statistical analysis

All data in this study were obtained from three independent experiments. Error bars indicate standard error of the mean (±s.e.m.). The data were analysed using a two-tailed Student's *t*-test with GraphPad Prism 9.0.0 software (https://www.graphpad.com/quickcalcs/ttest1/?format=SEM). Asterisks indicate significant statistical differences: ***$P \leq 0.001$, **$P \leq 0.01$ and *$P \leq 0.05$.

Accession numbers

Arabidopsis Genome Initiative (AGI) locus identifiers for the genes mentioned in this article are listed as follows: *MIR775A* (AT1G78206), *GALT9* (AT1G53290), *SAG12* (AT5G45890), *SAG29* (AT5G13170), *ORE1* (AT5G39610), *RBOHBD* (AT5G47910), *HY5* (AT5G11260), *EIN2* (AT5G03280), *EIN3* (AT3G20770) and *NCED3* (AT3G14440).

Acknowledgements

We acknowledge the National Institute of Plant Genome Research for providing necessary research facilities (plant growth facility, confocal/other microscopic facility and other central instrument facility) and internal grants. We also acknowledge the DBT-eLibrary Consortium (DeLCON) for providing access to e-resources.

Competing interests

The authors declare no competing or financial interests.

Author contributions

Conceptualization: A.K.S.; Methodology: V.M.; Software: A.K., V.M.; Validation: V.M., A.K.S.; Formal analysis: V.M., A.S., A.K.S.; Investigation: V.M., A.S., A.K.S.; Resources: A.K.S.; Data curation: V.M.; Writing - original draft: V.M., A.S.; Writing - review & editing: V.M., A.S., N.G., S.S.D., S.Y., A.K., A.K.S.; Visualization: V.M., A.S., N.G., S.S.D., S.Y., A.K., A.K.S.; Supervision: A.K.S., A.S.; Funding acquisition: A.K.S.

Funding

V.M. thanks the Department of Biotechnology (DBT), Ministry of Science and Technology, India (fellowship DBT/JRF/15/AL/223), A.S. thanks the Council of Scientific and Industrial Research, India (CSIR) [CSIR-SRA fellowship 13(9166-A)/2021-Pool], N.G. thanks the University Grants Commission (UGC) (fellowship 939/CSIR-UGC NET JUNE 2017), S.S.D. acknowledges the DBT (DBT-RA fellowship DBT/July/2020/22), A.K. thanks the CSIR [CSIR-SRA fellowship 13(9100-A)/2020-Pool). A.K.S. acknowledges the DBT for financial support (BT/PR12766/BPA/188/63/2015) and also support from National Institute of Plant Genome Research (NIPGR) and School of Life Sciences at Jawaharlal Nehru University (JNU), New Delhi.

References

Addo-Quaye, C., Miller, W. and Axtell, M. J. (2009). CleaveLand: a pipeline for using degradome data to find cleaved small RNA targets. *Bioinformatics (Oxford, England)* **25**, 130-131. doi:10.1093/bioinformatics/btn604

Ahmadizadeh, M., Chen, J.-T., Hasanzadeh, S., Ahmar, S. and Heidari, P. (2020). Insights into the genes involved in the ethylene biosynthesis pathway in Arabidopsis thaliana and Oryza sativa. *J. Genetic Eng. Biotechnol.* **18**, 1-20. doi:10.1186/s43141-020-00083-1

Ahmed, F., Rafii, M. Y., Ismail, M. R., Juraimi, A. S., Rahim, H. A., Asfaliza, R. and Latif, M. A. (2013). Waterlogging tolerance of crops: breeding, mechanism of tolerance, molecular approaches, and future prospects. *BioMed Res. Int.* **2013**, 963525. doi:10.1155/2013/963525

Allen, E., Xie, Z., Gustafson, A. M., Sung, G.-H., Spatafora, J. W. and Carrington, J. C. (2004). Evolution of microRNA genes by inverted duplication of target gene sequences in *Arabidopsis thaliana*. *Nat. Genet.* **36**, 1282-1290. doi:10.1038/ng1478

Bailey-Serres, J. and Voesenek, L. A. C. J. (2008). Flooding stress: acclimations and genetic diversity. *Annu. Rev. Plant Biol.* **59**, 313-339. doi:10.1146/annurev.arplant.59.032607.092752

Balazadeh, S., Siddiqui, H., Allu, A. D., Matallana-Ramirez, L. P., Caldana, C., Mehrnia, M., Zanor, M.-I., Köhler, B. and Mueller-Roeber, B. (2010). A gene regulatory network controlled by the NAC transcription factor ANAC092/AtNAC2/ORE1 during salt–promoted senescence. *Plant J.* **62**, 250-264. doi:10.1111/j.1365-313X.2010.04151.x

Barrero, J. M., Rodríguez, P. L., Quesada, V., Piqueras, P., Ponce, M. R. and Micol, J. L. (2006). Both abscisic acid (ABA)–dependent and ABA–independent pathways govern the induction of NCED3, AAO3 and ABA1 in response to salt stress. *Plant Cell Environ.* **29**, 2000-2008. doi:10.1111/j.1365-3040.2006.01576.x

Bengoa Luoni, S., Astigueta, F. H., Nicosia, S., Moschen, S., Fernandez, P. and Heinz, R. (2019). Transcription factors associated with leaf senescence in crops. *Plants (Basel)* **8**, 411. doi:10.3390/plants8100411

Bui, L. T., Shukla, V., Giorgi, F. M., Trivellini, A., Perata, P., Licausi, F. and Giuntoli, B. (2020). Differential submergence tolerance between juvenile and adult *Arabidopsis* plants involves the ANAC017 transcription factor. *Plant J.* **104**, 979-994. doi:10.1111/tpj.14975

Chen, X. (2009). Small RNAs and their roles in plant development. *Annu. Rev. Cell Dev. Biol.* **25**, 21-44. doi:10.1146/annurev.cellbio.042308.113417

Chen, L., Liao, B., Qi, H., Xie, L.-J., Huang, L., Tan, W.-J., Zhai, N., Yuan, L.-B., Zhou, Y., Yu, L.-J. et al. (2015). Autophagy contributes to regulation of the hypoxia response during submergence in *Arabidopsis thaliana*. *Autophagy* **11**, 2233-2246. doi:10.1080/15548627.2015.1112483

Crocker, W. J. (1932). The effect of ethylene upon living organisms. *Proc. Am. Philos. Soc.* **71**, 295-298.

Cui, J., You, C. and Chen, X. (2017). The evolution of microRNAs in plants. *Curr. Opin. Plant Biol.* **35**, 61-67. doi:10.1016/j.pbi.2016.11.006

Ding, S., Wang, L., Yang, Z., Lu, Q., Wen, X. and Lu, C. (2016). Decreased glutathione reductase2 leads to early leaf senescence in *Arabidopsis*. *J. Integr. Plant Biol.* **58**, 29-47. doi:10.1111/jipb.12371

Elstner, E. F. and Osswald, W. (1994). Mechanisms of oxygen activation during plant stress. *J. Plant Physiol.* **102**, 131-154. doi:10.1017/S0269727000014068

Fahlgren, N., Howell, M. D., Kasschau, K. D., Chapman, E. J., Sullivan, C. M., Cumbie, J. S., Givan, S. A., Law, T. F., Grant, S. R., Dangl, J. L. et al. (2007). High-throughput sequencing of *Arabidopsis* microRNAs: evidence for frequent birth and death of MIRNA genes. *PLoS ONE* **2**, e219. doi:10.1371/journal.pone.0000219

Fatland, B. L., Nikolau, B. J. and Wurtele, E. S. (2005). Reverse genetic characterization of cytosolic acetyl-CoA generation by ATP-citrate lyase in *Arabidopsis*. *Plant Cell* **17**, 182-203. doi:10.1105/tpc.104.026211

Franke, K. R., Schmidt, S. A., Park, S., Jeong, D.-H., Accerbi, M. and Green, P. J. (2018). Analysis of Brachypodium miRNA targets: evidence for diverse control during stress and conservation in bioenergy crops. *BMC Genomics* **19**, 547. doi:10.1186/s12864-018-4911-7

Fukao, T., Barrera-Figueroa, B. E., Juntawong, P. and Peña-Castro, J. M. (2019). Submergence and waterlogging stress in plants: a review highlighting research opportunities and understudied aspects. *Front. Plant Sci.* **10**. doi:10.3389/fpls.2019.00340

Gautam, V., Singh, A., Yadav, S., Singh, S., Kumar, P., Das, S. S. and Sarkar, A. K. (2020). Conserved LBL1-ta-siRNA and miR165/166-RLD1/2 modules regulate root development in maize. *Development* **148**, dev190033. doi:10.1242/dev.190033

Gille, S., Sharma, V., Baidoo, E., Keasling, J., Scheller, H. and Pauly, M. (2013). Arabinosylation of a Yariv-precipitable cell wall polymer impacts plant growth as exemplified by the *Arabidopsis* glycosyltransferase mutant ray1. *Mol. Plant* **6**, 1369-1372. doi:10.1093/mp/sst029

Glazińska, P., Wilmowicz, E., Wojciechowski, W., Frankowski, K. and Kopcewicz, J. (2014). Impact of InMIR319 and light on the expression of InTCP4 gene involved in the development of Ipomoea nil plants. *Acta Physiol. Plant.* **36**, 29-43. doi:10.1007/s11738-013-1384-9

Hiscox, J. D. and Israelstam, G. F. (1979). A method for the extraction of chlorophyll from leaf tissue without maceration. *Can. J. Bot.* **57**, 1332-1334. doi:10.1139/b79-163

Iqbal, N., Khan, N. A., Ferrante, A., Trivellini, A., Francini, A. and Khan, M. I. R. (2017). Ethylene role in plant growth, development and senescence: interaction with other phytohormones. *Front. Plant Sci.* **8**, 475. doi:10.3389/fpls.2017.00475

Ismail, A. M. (2018). Submergence tolerance in rice: resolving a pervasive quandary. *New Phytol.* **218**, 1298-1300. doi:10.1111/nph.15188

Jeong, D.-H., Schmidt, S. A., Rymarquis, L. A., Park, S., Ganssmann, M., German, M. A., Accerbi, M., Zhai, J., Fahlgren, N., Fox, S. E. et al. (2013). Parallel analysis of RNA ends enhances global investigation of microRNAs and target RNAs of Brachypodium distachyon. *Genome Biol.* **14**, R145. doi:10.1186/gb-2013-14-12-r145

Jiao, Q., Chen, T., Niu, G., Zhang, H., Zhou, C. and Hong, Z. (2020). N-glycosylation is involved in stomatal development by modulating the release of active abscisic acid and auxin in Arabidopsis. *J. Exp. Botany* **71**, 5865-5879. doi:10.1093/jxb/eraa321

Jin, S., Kanagaraj, A., Verma, D., Lange, T. and Daniell, H. (2011). Release of hormones from conjugates: chloroplast expression of β-glucosidase results in elevated phytohormone levels associated with significant increase in biomass and protection from aphids or whiteflies conferred by sucrose esters. *Plant Physiol.* **155**, 222-235. doi:10.1104/pp.110.160754

Jin, Q., Xu, Y., Mattson, N., Li, X., Wang, B., Zhang, X., Jiang, H., Liu, X., Wang, Y. and Yao, D. J. (2017). Identification of submergence-responsive microRNAs and their targets reveals complex miRNA-mediated regulatory networks in lotus (Nelumbo nucifera Gaertn). *Front. Plant Sci.* **8**, 6. doi:10.3389/fpls.2017.00006

Kang, J. S., Frank, J., Kang, C. H., Kajiura, H., Vikram, M., Ueda, A., Kim, S., Bahk, J. D., Triplett, B., Fujiyama, K. et al. (2008). Salt tolerance of *Arabidopsis thaliana* requires maturation of N-glycosylated proteins in the Golgi apparatus. *Proc. Natl. Acad. Sci. USA* **105**, 5933-5938. doi:10.1073/pnas.0800237105

Kim, J. H., Woo, H. R., Kim, J., Lim, P. O., Lee, I. C., Choi, S. H., Hwang, D. and Nam, H. G. (2009). Trifurcate feed-forward regulation of age-dependent cell death involving miR164 in *Arabidopsis*. *Science* **323**, 1053-1057. doi:10.1126/science.1166386

Kim, H. J., Hong, S. H., Kim, Y. W., Lee, I. H., Jun, J. H., Phee, B.-K., Rupak, T., Jeong, H., Lee, Y., Hong, B. S. et al. (2014). Gene regulatory cascade of senescence-associated NAC transcription factors activated by ETHYLENE-INSENSITIVE2-mediated leaf senescence signalling in *Arabidopsis*. *J. Exp. Bot.* **65**, 4023-4036. doi:10.1093/jxb/eru112

Kim, J., Chang, C. and Tucker, M. L. (2015a). To grow old: regulatory role of ethylene and jasmonic acid in senescence. *Front. Plant Sci.* **6**. doi:10.3389/fpls.2015.00020

Kim, S.-J., Held, M. A., Zemelis, S., Wilkerson, C. and Brandizzi, F. J. (2015b). CGR 2 and CGR 3 have critical overlapping roles in pectin methylesterification and plant growth in *Arabidopsis thaliana*. *Plant J.* **82**, 208-220. doi:10.1111/tpj.12802

Kraehmer, H. (2016). *Morphological adaptation to water*. In *Atlas of Weed Mapping*, pp. 192-193. Wiley. doi:10.1002/9781118720691.ch25

Kumar, A. and Dash, P. K. (2019). Transcriptome analysis for abiotic stresses in rice (Oryza sativa L.). In *Transcriptome Analysis*. IntechOpen. doi: 10.5772/intechopen.84955

Larkin, M. A., Blackshields, G., Brown, N. P., Chenna, R., McGettigan, P. A., McWilliam, H., Valentin, F., Wallace, I. M., Wilm, A., Lopez, R. et al. (2007). Clustal W and Clustal X version 2.0. *Bioinformatics* **23**, 2947-2948. doi:10.1093/bioinformatics/btm404

Lee, K. H., Piao, H. L., Kim, H.-Y., Choi, S. M., Jiang, F., Hartung, W., Hwang, I., Kwak, J. M., Lee, I.-J. and Hwang, I. J. C. (2006). Activation of glucosidase via stress-induced polymerization rapidly increases active pools of abscisic acid. *Cell* **126**, 1109-1120. doi:10.1016/j.cell.2006.07.034

Li, W. and Lan, P. (2017). The understanding of the plant iron deficiency responses in strategy I plants and the role of ethylene in this process by omic approaches. *Front. Plant Sci.* **8**. doi:10.3389/fpls.2017.00040

Li, G., Deng, Y., Geng, Y., Zhou, C., Wang, Y., Zhang, W., Song, Z., Gao, L. and Yang, J. (2017). Differentially expressed microRNAs and target genes associated with plastic internode elongation in Alternanthera philoxeroides in contrasting hydrological habitats. *Front. Plant Sci.* **8**, 2078. doi:10.3389/fpls.2017.02078

Licausi, F., Weits, D. A., Pant, B. D., Scheible, W.-R., Geigenberger, P. and van Dongen, J. (2011). Hypoxia responsive gene expression is mediated by various subsets of transcription factors and miRNAs that are determined by the actual oxygen availability. *Front. Plant Sci.* **190**, 442-456. doi:10.1111/j.1469-8137.2010.03451.x

Liu, Z.-J., Guo, Y.-K. and Bai, J.-G. (2010). Exogenous hydrogen peroxide changes antioxidant enzyme activity and protects ultrastructure in leaves of two cucumber ecotypes under osmotic stress. *J. Plant Growth Regul.* **29**, 171-183. doi:10.1007/s00344-009-9121-8

Liu, Z., Kumari, S., Zhang, L., Zheng, Y. and Ware, D. (2012). Characterization of miRNAs in response to short-term waterlogging in three inbred lines of Zea mays. *PLoS ONE* **7**, e39786. doi:10.1371/journal.pone.0039786

Loreti, E. and Striker, G. G. (2020). Plant responses to hypoxia: signaling and adaptation. *Plants (Basel)* **9**, 1704. doi:10.3390/plants9121704

Lu, S. (2019). De novo origination of MIRNAs through generation of short inverted repeats in target genes. *RNA Biol.* **16**, 846-859. doi:10.1080/15476286.2019.1593744

Lu, C., Kulkarni, K., Souret, F. F., MuthuValliappan, R., Tej, S. S., Poethig, R. S., Henderson, I. R., Jacobsen, S. E., Wang, W., Green, P. J. et al. (2006). MicroRNAs and other small RNAs enriched in the *Arabidopsis* RNA-dependent RNA polymerase-2 mutant. *Genome Res.* **16**, 1276-1288. doi:10.1101/gr.5530106

Mishra, P., Singh, A., Verma, A. K., Singh, R. and Roy, S. J. B. (2021). microRNA775 targets a β-(1, 3)-galactosyltransferase to regulate growth and development in *Arabidopsis thaliana*. *J. Plant Growth Regul.* doi:10.1007/s00344-021-10511-2

Moldovan, D., Spriggs, A., Yang, J., Pogson, B. J., Dennis, E. S. and Wilson, I. W. (2010). Hypoxia-responsive microRNAs and trans-acting small interfering RNAs in *Arabidopsis*. *J. Exp. Bot.* **61**, 165-177. doi:10.1093/jxb/erp296

Murashige, T. and Skoog, F. (1962). A revised medium for rapid growth and bio assays with tobacco tissue cultures. *Physiol. Plant* **15**, 473-497. doi:10.1111/j.1399-3054.1962.tb08052.x

Nagashima, Y., von Schaewen, A. and Koiwa, H. (2018). Function of N-glycosylation in plants. *Plant Sci.* **274**, 70-79. doi:10.1016/j.plantsci.2018.05.007

Nakamura, M. and Noguchi, K. (2020). Tolerant mechanisms to O 2 deficiency under submergence conditions in plants. *J. Plant Res. 1-29* **133**, 343-371. doi:10.1007/s10265-020-01176-1

Neljubow, D. (1901). Uber die horizontale Nutation der Stengel von Pisum Sativum und einiger anderen Planzen. *Bot. Centralbl. Beih.* **10**, 128-139.

Nishiuchi, S., Yamauchi, T., Takahashi, H., Kotula, L. and Nakazono, M. (2012). Mechanisms for coping with submergence and waterlogging in rice. *Rice* **5**, 2. doi:10.1186/1939-8433-5-2

Ostrowski, M. and Jakubowska, A. (2014). UDP-glycosyltransferases of plant hormones. *Adv. Cell Biol.* **4**, 43-60. doi:10.2478/acb-2014-0003

Qiao, H., Chang, K. N., Yazaki, J. and Ecker, J. R. (2009). Interplay between ethylene, ETP1/ETP2 F-box proteins, and degradation of EIN2 triggers ethylene responses in Arabidopsis. *Genes Dev.* **23**, 512-521. doi:10.1101/gad.1765709

Qin, L.-X., Rao, Y., Li, L., Huang, J.-F., Xu, W.-L. and Li, X.-B. (2013). Cotton GalT1 encoding a putative glycosyltransferase is involved in regulation of cell wall pectin biosynthesis during plant development. *PLoS ONE* **8**, e59115. doi:10.1371/journal.pone.0059115

Qiu, K., Li, Z., Yang, Z., Chen, J., Wu, S., Zhu, X., Gao, S., Gao, J., Ren, G. and Kuai, B. (2015). EIN3 and ORE1 accelerate degreening during ethylene-mediated leaf senescence by directly activating chlorophyll catabolic genes in *Arabidopsis*. *PLoS Genet.* **11**, e1005399. doi:10.1371/journal.pgen.1005399

Qu, Y., Egelund, J., Gilson, P. R., Houghton, F., Gleeson, P. A., Schultz, C. J. and Bacic, A. (2008). Identification of a novel group of putative *Arabidopsis thaliana* β-(1, 3)-galactosyltransferases. *Plant Mol. Biol.* **68**, 43-59. doi:10.1007/s11103-008-9351-3

Qu, G., Kruszka, K., Plewka, P., Yang, S.-Y., Chiou, T.-J., Jarmolowski, A., Szweykowska-Kulinska, Z., Echeverria, M. and Karlowski, W. M. (2015). Promoter-based identification of novel non-coding RNAs reveals the presence of dicistronic snoRNA-miRNA genes in Arabidopsis thaliana. *BMC Genomics* **16**, 1009. doi:10.1186/s12864-015-2221-x

Rajagopalan, R., Vaucheret, H., Trejo, J. and Bartel, D. P. (2006). A diverse and evolutionarily fluid set of microRNAs in *Arabidopsis thaliana*. *Genes Dev.* **20**, 3407-3425. doi:10.1101/gad.1476406

Richardson, A. D., Duigan, S. P. and Berlyn, G. P. (2002). An evaluation of noninvasive methods to estimate foliar chlorophyll content. *New Phytol.* **153**, 185-194. doi:10.1046/j.0028-646X.2001.00289.x

Roy, A., Kucukural, A. and Zhang, Y. (2010). I-TASSER: a unified platform for automated protein structure and function prediction. *Nat. Protoc.* **5**, 725-738. doi:10.1038/nprot.2010.5

Schwarz, F. and Aebi, M. (2011). Mechanisms and principles of N-linked protein glycosylation. *Curr. Opin. Struct. Biol.* **21**, 576-582. doi:10.1016/j.sbi.2011.08.005

Seo, P. J., Park, J.-M., Kang, S. K., Kim, S.-G. and Park, C.-M. (2011). An *Arabidopsis* senescence-associated protein SAG29 regulates cell viability under high salinity. *Planta* **233**, 189-200. doi:10.1007/s00425-010-1293-8

Singh, S., Singh, A., Yadav, S., Gautam, V., Singh, A. and Sarkar, A. K. (2017). Sirtinol, a Sir2 protein inhibitor, affects stem cell maintenance and root development in *Arabidopsis thaliana* by modulating auxin-cytokinin signaling components. *Sci. Rep.* **7**, 42450. doi:10.1038/srep42450

Singh, A., Gandhi, N., Mishra, V., Yadav, S., Rai, V. and Sarkar, A. K. (2020a). Role of abiotic stress responsive miRNAs in *Arabidopsis* root development. *J. Plant Biochem. Biotechnol.* **29**, 733-742. doi:10.1007/s13562-020-00626-0

Singh, S., Yadav, S., Singh, A., Mahima, M., Singh, A., Gautam, V. and Sarkar, A. K. (2020b). Auxin signaling modulates LATERAL ROOT PRIMORDIUM1 (LRP1) expression during lateral root development in *Arabidopsis*. *Plant J.* **101**, 87-100. doi:10.1111/tpj.14520

Smirnoff, N. (1995). *Environment and Plant Metabolism: Flexibility and Acclimation*. BIOS Scientific publishers.

Tamang, B. and Fukao, T. (2015). Plant adaptation to multiple stresses during submergence and following desubmergence. *Int. J. Mol. Sci.* **16**, 30164-30180. doi:10.3390/ijms161226226

Todesco, M., Rubio-Somoza, I., Paz-Ares, J. and Weigel, D. (2010). A collection of target mimics for comprehensive analysis of microRNA function in *Arabidopsis thaliana*. *PLoS Genet.* **6**, e1001031. doi:10.1371/journal.pgen.1001031

Tripathi, A. M., Singh, A., Singh, R., Verma, A. K. and Roy, S. (2019). Modulation of miRNA expression in natural populations of A. thaliana along a wide altitudinal gradient of Indian Himalayas. *Sci. Rep.* **9**, 441. doi:10.1038/s41598-018-37465-y

Ueda, H., Ito, T., Inoue, R., Masuda, Y., Nagashima, Y., Kozuka, T. and Kusaba, M. J. (2020). Genetic interaction among phytochrome, ethylene and abscisic acid signaling during dark-induced senescence in *Arabidopsis thaliana*. *Front. Plant Sci.* **11**. doi:10.3389/fpls.2020.00564

Varkonyi-Gasic, E., Wu, R., Wood, M., Walton, E. F. and Hellens, R. P. (2007). Protocol: a highly sensitive RT-PCR method for detection and quantification of microRNAs. *Plant Methods* **3**, 12. doi:10.1186/1746-4811-3-12

Visser, E. J. W., Voesenek, L. A. C. J., Vartapetian, B. B. and Jackson, M. B. (2003). Flooding and plant growth. *Ann. Bot.* **91**, 107-109. doi:10.1093/aob/mcg014

Voinnet, O. (2009). Origin, biogenesis, and activity of plant microRNAs. *Cell.* **136**, 669-687. doi:10.1016/j.cell.2009.01.046

von Schaewen, A., Frank, J. and Koiwa, H. J. (2008). Role of complex N-glycans in plant stress tolerance. *Plant Signal Behav.* **3**, 871-873. doi:10.4161/psb.3.10.6227

Wang, H., Wang, J., Jiang, J., Chen, S., Guan, Z., Liao, Y. and Chen, F. (2014). Reference genes for normalizing transcription in diploid and tetraploid *Arabidopsis*. *Sci. Rep.* **4**, 6781. doi:10.1038/srep06781

Wang, Z., Feng, Y., Li, J., Zou, J. and Fan, L. (2020). Integrative microRNA and mRNA analysis reveals regulation of ER stress in the Pacific white shrimp Litopenaeus vannamei under acute cold stress. *Comp. Biochem. Physiol. D Genomics Proteomics* **33**, 100645. doi:10.1016/j.cbd.2019.100645

Wang, C., Dai, S., Zhang, Z. L., Lao, W., Wang, R., Meng, X. and Zhou, X. (2021). Ethylene and salicylic acid synergistically accelerate leaf senescence in *Arabidopsis*. *J. Integr. Plant Biol.* **63**, 828-833. doi:10.1111/jipb.13075

Weaver, L. M., Gan, S., Quirino, B. and Amasino, R. M. (1998). A comparison of the expression patterns of several senescence-associated genes in response to stress and hormone treatment. *Plant Mol. Biol.* **37**, 455-469. doi:10.1023/A:1005934428906

Xiong, L., Lee, H., Ishitani, M. and Zhu, J.-K. (2002). Regulation of osmotic stress-responsive gene expression by thelos6/aba1 locus in *Arabidopsis*. *J. Biol. Chem.* **277**, 8588-8596. doi:10.1074/jbc.M109275200

Yamauchi, T., Shimamura, S., Nakazono, M. and Mochizuki, T. (2013). Aerenchyma formation in crop species: A review. *Field Crops Res.* **152**, 8-16. doi:10.1016/j.fcr.2012.12.008

Yang, J., Yan, R., Roy, A., Xu, D., Poisson, J. and Zhang, Y. (2015). The I-TASSER Suite: protein structure and function prediction. *Nat. Methods* **12**, 7-8. doi:10.1038/nmeth.3213

Yeung, E., van Veen, H., Vashisht, D., Sobral Paiva, A. L., Hummel, M., Rankenberg, T., Steffens, B., Steffen-Heins, A., Sauter, M., de Vries, M. et al. (2018). A stress recovery signaling network for enhanced flooding tolerance in *Arabidopsis thaliana*. *Proc. Natl. Acad. Sci. USA* **115**, E6085-E6094. doi:10.1073/pnas.1803841115

Zhai, L., Liu, Z., Zou, X., Jiang, Y., Qiu, F., Zheng, Y. and Zhang, Z. (2013). Genome–wide identification and analysis of microRNA responding to long–term waterlogging in crown roots of maize seedlings. *Physiol. Plant.* **147**, 181-193. doi:10.1111/j.1399-3054.2012.01653.x

Zhang, Y. (2008). I-TASSER server for protein 3D structure prediction. *BMC Bioinformatics* **9**, 40. doi:10.1186/1471-2105-9-40

Zhang, J., Van Toai, T., Huynh, L. and Preiszner, J. (2000). Development of flooding-tolerant *Arabidopsis thaliana* by autoregulated cytokinin production. *Mol. Breed.* **6**, 135-144. doi:10.1023/A:1009694029297

Zhang, B., Pan, X., Cannon, C. H., Cobb, G. P. and Anderson, T. A. (2006). Conservation and divergence of plant microRNA genes. *Plant J.* **46**, 243-259. doi:10.1111/j.1365-313X.2006.02697.x

Zhang, Z., Wei, L., Zou, X., Tao, Y., Liu, Z. and Zheng, Y. (2008). Submergence-responsive microRNAs are potentially involved in the regulation of morphological and metabolic adaptations in maize root cells. *Ann Bot.* **102**, 509-519. doi:10.1093/aob/mcn129

Zhang, H., He, H., Wang, X., Wang, X., Yang, X., Li, L. and Deng, X. W. (2011). Genome-wide mapping of the HY5-mediated gene networks in *Arabidopsis* that involve both transcriptional and post-transcriptional regulation. *Plant J.* **65**, 346-358. doi:10.1111/j.1365-313X.2010.04426.x

Zhang, C., Teng, X.-D., Zheng, Q.-Q., Zhao, Y.-Y., Lu, J.-Y., Wang, Y., Guo, H. and Yang, Z.-N. (2018). Ethylene signaling is critical for synergid cell functional specification and pollen tube attraction. *Plant J.* **96**, 176-187. doi:10.1111/tpj.14027

Zhang, H., Guo, Z., Zhuang, Y., Suo, Y., Du, J., Gao, Z., Pan, J., Li, L., Wang, T., Xiao, L. J. et al. (2021). MicroRNA775 regulates intrinsic leaf size and reduces cell wall pectin levels by targeting a Galactosyltransferase gene in *Arabidopsis*. *Plant Cell* **33**, 581-602. doi:10.1093/plcell/koaa049